

**Fingerprint Matching using Moments and Moment
Invariants**

BY

Waleed Mohammad Alzahrani

A Thesis Presented to the
DEANSHIP OF GRADUATE STUDIES

KING FAHD UNIVERSITY OF PETROLEUM & MINERALS

DHAHRAN, SAUDI ARABIA

In Partial Fulfillment of the
Requirements for the Degree of

MASTER OF SCIENCE

In

COMPUTER SCIENCE

2010

King Fahd University of Petroleum & Minerals

Dhahran 31261, Saudi Arabia

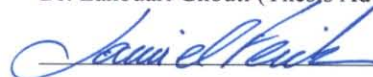
Deanship of graduate Studies

This thesis, written by **WALEED MOHAMMAD K. ALKENANI ALZAHIRANI** under the direction of his thesis advisor and approved by his thesis committee, has been presented to and accepted by the Dean of Graduate Studies, in partial fulfillment of his requirements for the degree of **MASTER OF SCIENCE IN COMPUTER SCIENCE**.

THEISIS COMMITTEE



Dr. Lahouari Ghouti (Thesis Advisor)



Dr. Sami Elferik (Member)



Dr. Wasfi G. Al-Khatib (Member)



Dr. Adel Fadhl Ahmed
Department Chirman



Dr. Salam A. Zummo
Dean of Graduate Studies

29/11/10

Date



I would like to dedicate my thesis to
My parents
who taught me the value of knowledge
and my brother and sisters

ACKNOWLEDGMENT

To my family for their support and understanding while I was busy and spending long hours during my course of study.

My sincere thanks also go to Dr. Lahouari Ghouti, my advisor, for his most valuable insights, generous and patient help on my work. His intellectual guidance is priceless, not to mention his policy of having an open door for discussions and giving endless encouragement. I am also grateful to my thesis committee members, Dr. Sami Elferik and Dr. Wasfi G. Al-Khatib, for their valuable suggestions and comments.

TABLE OF CONTENTS

	Page
TABLE OF CONTENTS	iv
LIST OF TABLES	vii
LIST OF FIGURES	viii
THESIS ABSTRACT.....	x
ملخص الرسالة.....	xi
CHAPTER 1	1
1. INTRODUCTION	1
1.1 Biometrics.....	3
1.1.1 Properties of biometric traits	6
1.2 Fingerprint as a Biometric	7
1.3 Thesis Motivation	10
1.4 Problem Statement	11
1.5 Outline of the Thesis.....	12
CHAPTER 2	14
2. OVERVIEW OF FINGERPRINT-BASED BIOMETRIC SYSTEMS	14
2.1 Fingerprint Acquisition	14
2.2 System Functionalities.....	17
2.3 Fingerprint Representation and Feature Extraction.....	19
2.4 Fingerprint Preprocessing.....	21
2.4.1 Fingerprint Segmentation.....	21

2.4.2	Fingerprint Enhancement	23
2.4.3	Fingerprint Binarization/Skeletonization.....	24
2.5	Performance Measures	25
2.6	Benchmark Databases	29
CHAPTER 3		32
3.	RELATED WORK	32
3.1	Fingerprint Verification Methods	32
3.1.1	Minutiae based Approach	33
3.1.2	Correlation based Approach.....	34
3.1.3	Ridge Features (Texture) based Approach	34
3.1.4	Transform-Based based Approach	37
CHAPTER 4		39
4.	MATHEMATICAL BACKGROUND.....	39
4.1	Scale Invariant Feature Transform SIFT.....	39
4.2	Discrete Wavelets.....	43
4.3	Directional Wavelets and Filters.....	46
4.4	Filter Banks	47
5.5	Directional Filter Bank	50
4.6	Curvelets.....	54
4.7	Invariants	55
4.7.1	Categories of Invariants.....	56
4.8	Moments	57
4.9	Moment Invariants to Translation, Rotation and Scaling.....	60
4.10	Affine Moment Invariants	61
4.10.1	Dependencies Among the AMIs	63

CHAPTER 5	65
5. PROPOSED FINGERPRINT MATCHING ALGORITHM	65
5.1 Directional Filtering and Feature Extraction	65
5.2 Image Normalization	67
5.3 Reference Point and Region of Interest	68
4.3.1 Determination of Reference point	68
4.3.2 Determination of ROI and Partition.....	69
5.4 Invariant Moment Feature Vector Generation	71
5.5 Fingerprint Matching.....	72
CHAPTER 6	74
6. EXPERIMENTAL RESULTS	74
CHAPTER 7	81
7. CONCLUSION	81
7.1 Overview.....	81
7.2 Summary of Contributions	82
7.3 Future Work.....	83
8. REFERENCES.....	84
Vita.....	89

LIST OF TABLES

Table 1.1: Comparison of commonly used biometric traits. High, Medium, and Low are denoted by H, M, and L, respectively [5].	7
Table 2.1: FVC2002 Fingerprint Database [12].	30
Table 4.1: Hu moments & Rotation Invariants.	59
Table 6.1: Number of Tests.	74
Table 6.2: Statistical characteristics of genuine and imposter distributions (DB1_A).	76
Table 6.3: Testing results.	77
Table 6.4: Time & memory comparison.	80

LIST OF FIGURES

Figure 1.1: Annual Biometric Industry Revenues (in US \$ millions).	3
Figure 1.2: Expected growth in revenues of biometrics industry (in US \$ millions) [4].	4
Figure 1.3: Examples of biometrics traits: a) ear, b) face, c) facial thermogram, d) hand thermogram) hand vein, f) hand geometry, g) fingerprint, h) iris, i) retina, j) signature, and k) voice [5].	5
Figure 1.4: Revenue by biometric technology as estimated by the International Biometric Group [3].	6
Figure 1.5: Fingerprint Classes.	8
Figure 1.6: An illustration of minutiae points	9
Figure 2.1: Fingerprint scanners/readers	15
Figure 2.2: FTIR-based fingerprint sensor operation [5]	16
Figure 2.3: Fingerprint system functionalities.	18
Figure 2.4: Ridge ending and ridge bifurcation.	19
Figure 2.5: Core and delta.	20
Figure 2.6: (a) original image (b) image with segmentation.	22
Figure 2.7: (a) original image (b) enhanced image using FFT.	24
Figure 2.8: (a) gray-scale image (b) binarized image (c) skeleton image obtained after a thinning of the image in (b) [5].	25
Figure 2.9: ROC curve is a plot of the true positive rate against the false positive rate for the different possible thresholds.	27
Figure 2.10: FAR and FRR for a given threshold (t), displayed over the genuine and impostor score distributions.	28
Figure 2.11: FVC2002 fingerprint database example [12].	30
Figure 3.1: Texture Based matching Using a Filter-Bank of Gabor filters [15].	35
Figure 3.2: DFB illustration, Frequency partition map of (a) the input and (b) the eight sub-band outputs. (c) Example of fingerprint image. (d) Decomposed sub-band outputs of (c) using eight-band DFB.	36
Figure 4.1: Scale space construction for SIFT operation [6].	42
Figure 4.2: Difference between cosine wave and wavelet.	43
Figure 4.3: Wavelet Decomposed Fingerprint.	44
Figure 4.4: Coherence images: (a) Approximate image, (b, c) Horizontal, Vertical details.	45
Figure 4.5: Reference point (X), and region of interest divided into 80 sectors imposed on the fingerprint.	48
Figure 4.6: Directional filter bank frequency partitioning [39].	48
Figure 4.7: Directional image [25].	50
Figure 4.8: First phase of an eight-band DFB.	51
Figure 4.9: Second phase of an eight-band DFB.	52
Figure 4.10: Third phase of an eight-band DFB.	53
Figure 4.11: Wavelet vs. Curvelet [42].	54

Figure 4.12: Rotated fingerprint example.....	59
Figure 5.1: blocks in (a) Original image, (b) Sub-band output.	66
Figure 5.2: The reference point one on the convex ridge.	68
Figure 5.3: Region of interest (ROI) for feature extraction. A sample fingerprint (a) whose ROI is established within the image and (b) whose ROI exceeds the image bound.	70
Figure 6.1: Genuine and imposter distributions for the proposed method (DB1_A).	75
Figure 6.2: ROC curves comparing the recognition rate performance of the proposed method with the other 2 methods on database FVC2002 DB1_A.....	78
Figure 6.3: ROC curves on database FVC2002 DB2_A.....	78
Figure 6.4: ROC curves on database FVC2002 DB3_A.....	79
Figure 6.5: ROC curves on database FVC2002 DB4_A.....	79

THESIS ABSTRACT

Name: Waleed Mohammad Alzahrani
Title: Fingerprint Matching using Moments and Moment Invariants
Major Field: Information and Computer Science
Date of Degree: November 2010

Fingerprints represent the most common biometric trait in use today in various applications ranging from person identification to access control. The search for better performance in matching and recognition has been the focus of ongoing research efforts in this fast evolving field. Advanced matching algorithms using state-of-the-art image processing techniques have emerged in the recent literature. This thesis constitutes the outcome of similar efforts. Unlike minutia-based techniques, in this thesis, we propose a fingerprint matching technique that combines directional features with moment invariants. The main attribute of the proposed scheme is its ability to bypass the need for translation and rotation alignments usually carried out through computationally-demanding registration techniques. The performance of the proposed fingerprint matching algorithm is evaluated using benchmark fingerprint databases FVC2002. Reported results clearly indicate the superiority of the proposed scheme.

ملخص الرسالة

الاسم:	وليد بن محمد بن خير الله الكناني الزهراني
عنوان الرسالة:	مطابقة بصمات اليد باستخدام العزم الرقمي للصور و الثوابت العزمية
التخصص:	علوم الحاسب الآلي
تاريخ التخرج:	ذو القعدة 1431 هـ

تعتبر البصمات السمة الأكثر استخداماً في أنظمة التعرف الحيوية اليوم في مختلف التطبيقات، مثل التعرف على هوية الشخص وأنظمة التحكم في العبور. وما زال البحث عن أداء أفضل في التحقق والتعرف هو محل الاهتمام والموجه لجهود البحث الجارية في هذا المجال سريع التطور. وفي خلال العقد المنصرم ظهرت خوارزميات متقدمة باستخدام أحدث تقنيات معالجة الصور، وهذه الرسالة تشكل نتائج جهود مماثلة ولكن بعكس التقنيات المعتمدة على نقاط التعرف (minutia)، ففي هذه الرسالة نقترح تقنية مطابقة للبصمات تجمع بين السمات المتجهة والثوابت العزمية. السمة الرئيسية للخوارزمية المقترحة هي عدم حاجتها لعمليات المحاذاة للدوران والضبط والتي عادة ما تتطلب حسابات عالية التعقيد بسبب احتياجها إلى تقنيات التسجيل التصويرية. وتم تقييم أداء خوارزمية مطابقة البصمات المقترحة باستخدام قواعد بيانات بصمات الأصابع FVC2002. وأظهرت الدراسة تميزاً ملحوظاً في كفاءة التعرف مقارنة بالطرق التقليدية.

CHAPTER 1

1. INTRODUCTION

In an increasingly digital world, personal identity is becoming a significant issue in enabling secured access to physical and digital assets and resources. Existing security measures can be classified into knowledge-based and token-based approaches. While the former rely on passwords, the access cards are used in the latter approaches to control access to physical and virtual (mainly digital) facilities.

Both approaches are known to suffer from several limitations. Forgetting the passwords and losing access cards is very common. Access cards (smart or passive) can be stolen, forged, lost or spoofed. Also, passwords are vulnerable to dictionary and brute force attacks. Biometric systems using fingerprint, face and voice recognition avoid such limitations and offer means for reliable personal authentication that can address these problems.

Moreover, due to their cost-effectiveness, biometric systems are gaining wide acceptance in many day-to-day civilian, government, and military

applications. In fact, several countries are resorting to biometric-based solutions to control access to their borders. It is worth noting also that using biometric-based identification, an individual cannot simply disassociate himself/herself, for example, from an online banking transaction by claiming that his password or card was stolen. This property is referred to as *non-repudiation* [1].

Building on their successful use in forensic applications by law enforcement agencies to solve crime investigations, fingerprints have found their way to the digital world, thanks to efficient storage; compression and transmission of their digitized representations.

Although face, iris and other biometric traits have proven to be effective features for biometric identification, fingerprints continue to be an attractive means for person identification and verification due to the availability of cheap scanning devices based on different technologies, efficient feature extraction mechanisms in several domains and spaces (spatial and transform) and fast matching procedures. Unlike what is commonly believed and despite active research in fingerprint recognition and matching over several years, the search for reliable, yet efficient and fast, fingerprint recognition schemes is still an open problem.

1.1 Biometrics

Biometric recognition, or biometrics, refers to the science of automatic identification of a person based on his/her anatomical (e.g., fingerprint, iris, ..., etc.) or behavioral (e.g., signature) characteristics. This field has been a research focus in both academia and industry. Figure 1.1 shows the annual biometric industry revenues from 2005 to 2010 [2]. Figure 1.1 clearly reflects the trend in adopting biometric-based person identification and verification solutions.

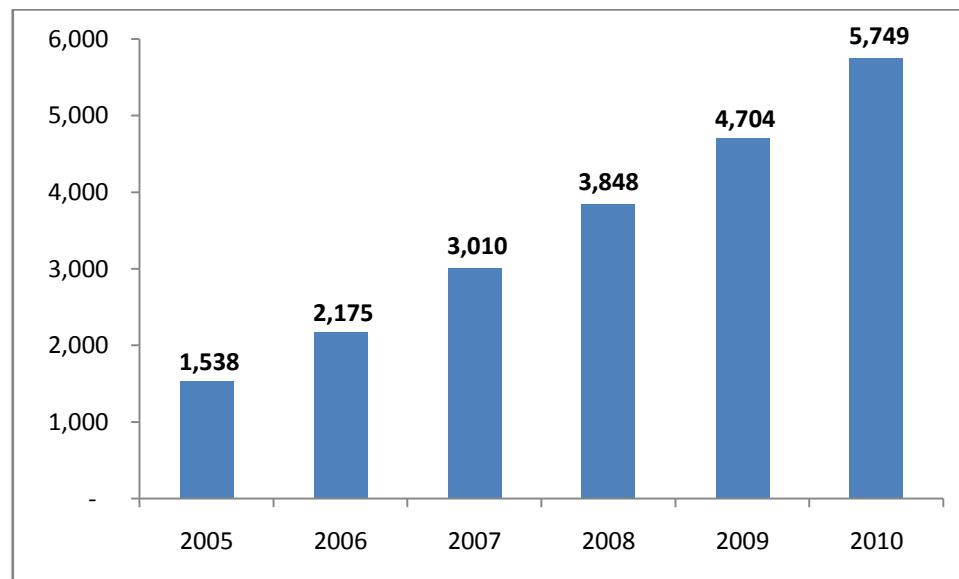


Figure 1.1: Annual Biometric Industry Revenues (in US \$ millions).

Biometrics industry is forecasted to grow rapidly in the upcoming years as shown in Figure 1.2 [3]. It is expected that such steady growth will not be

significantly impacted by the 2008 global economic meltdown. Also, the biometrics industry is expected to remain on track to experience significant growth through 2017 and beyond reaching nearly US \$ 11 Billion in annual revenues by 2017 [4].

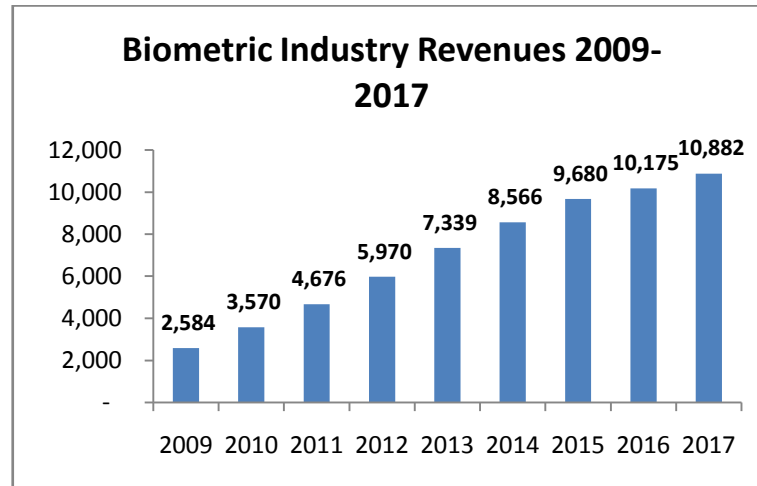


Figure 1.2: Expected growth in revenues of biometrics industry (in US \$ millions) [4].

A number of biometric traits have been developed and are used to authenticate a person's identity. The key idea resides in using special characteristics of a person for identification purposes. Such special characteristics include face, iris, fingerprint, signature, etc. Figure 1.3 gives an illustration of different biometric features currently in use for various applications and purposes.

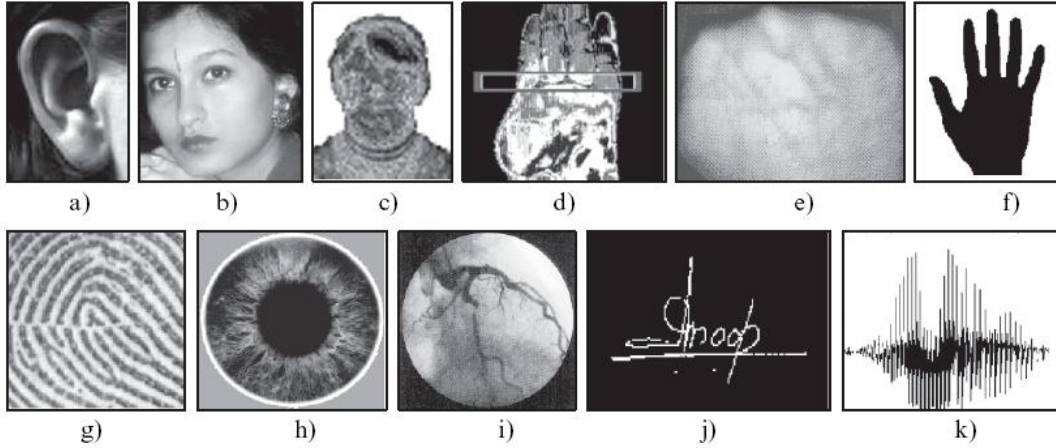


Figure 1.3: Examples of biometrics traits: a) ear, b) face, c) facial thermogram, d) hand thermogram, e) hand vein, f) hand geometry, g) fingerprint, h) iris, i) retina, j) signature, and k) voice [5].

Various biometric traits are being used for real-time recognition. The most popular traits are being face, iris and fingerprint. In some applications, more than one biometric trait is used to attain higher security and to handle failure to enroll situations for some users. Such systems are called *multimodal biometric systems* [1]. However, in this thesis, only fingerprint-based systems are considered. Several reasons are behind such a choice. The maturity of fingerprint-based systems represents the major reason behind the choice made in this thesis. Additionally, fingerprint-based systems continue to be the leading biometric technology in terms of market share as shown in Figure 1.4.

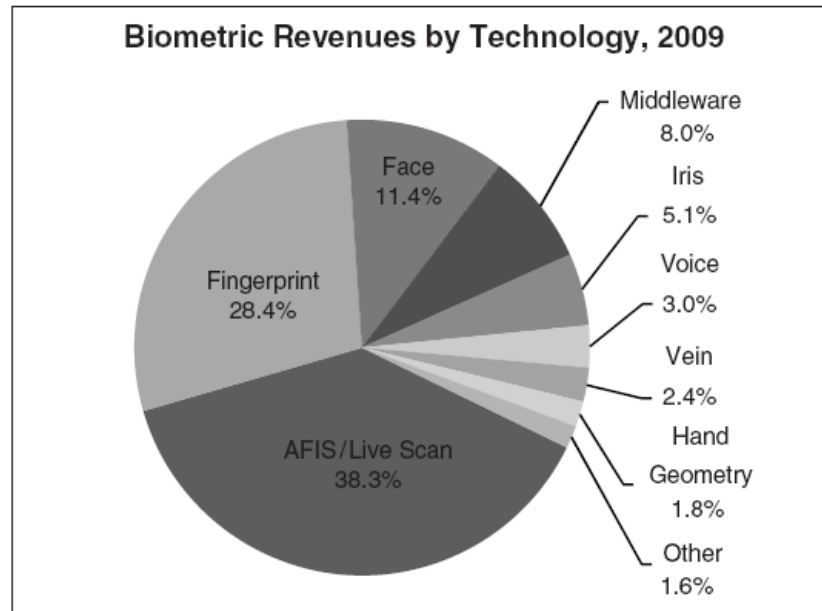


Figure 1.4: Revenue by biometric technology as estimated by the International Biometric Group [3].

1.1.1 Properties of biometric traits

For a human characteristic to be used for biometrics, it should have posses desirable properties [1]:

- **Universality:** each person should have the characteristic.
- **Uniqueness:** how well the biometric separates an individual from another.
- **Permanence:** measures how well a biometric resists aging and other types of changes over time.
- **Collectability:** ease of acquisition for measurement.
- **Performance:** accuracy, speed, and robustness of technology used.
- **Acceptability:** degree of approval of a technology.
- **Circumvention:** ease of use of a substitute.

The biometric identifiers described above are compared in Table 1.1. Note that fingerprint has a nice balance among all the desirable properties. Also, keep in mind that fingerprints are very distinctive and they are permanent; even if they temporarily change slightly due to cuts and bruises on the skin, the fingerprint reappears after the finger heals.

Biometric identifier	Universality	Distinctiveness	Permanence	Collectability	Performance	Acceptability	Circumvention
Face	H	L	M	H	L	H	H
Fingerprint	M	H	H	M	H	M	M
Hand geometry	M	M	M	H	M	M	M
Hand/finger vein	M	M	M	M	M	M	L
Iris	H	H	H	M	H	L	L
Signature	L	L	L	H	L	H	H
Voice	M	L	L	M	L	H	H

Table 1.1: Comparison of commonly used biometric traits. High, Medium, and Low are denoted by H, M, and L, respectively [5].

1.2 Fingerprint as a Biometric

A fingerprint is believed to be unique to each person (and each finger). Fingerprints of even identical twins are different. Fingerprints are one of the most mature biometric technologies and are considered legitimate proofs of evidence in courts of law all over the world. Fingerprints are, therefore, used

in forensic divisions worldwide for criminal investigations. More recently, an increasing number of civilian and commercial applications are either using or actively considering using fingerprint-based identification because of a better understanding of fingerprints as well as demonstrated matching performance than any other existing biometric technology.

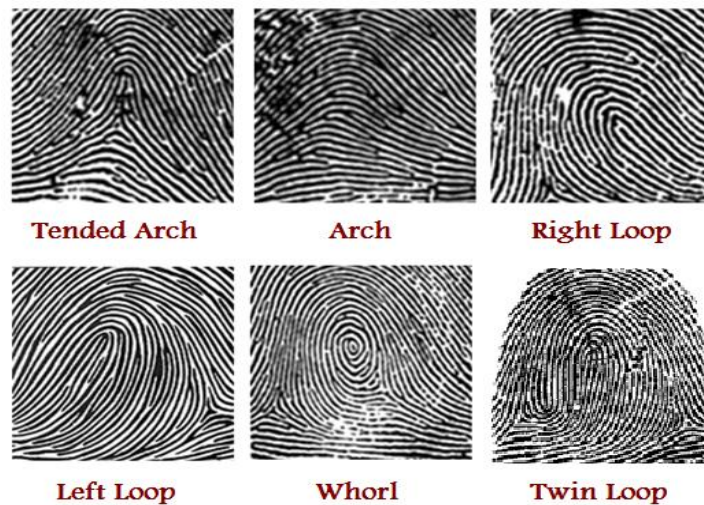


Figure 1.5: Fingerprint Classes

The most popular method for fingerprint representation is based on local landmarks called minutiae points. This scheme evolved from an intuitive system design tailored by the needs of forensic experts who visually classify the fingerprint into one of six categories [5]: arch, tented arch, right loop, left loop, whorl, and twin loop. The fingerprints images shown in Figure 1.5 illustrate those six categories. Minutiae-based systems first locate the minutiae points in fingerprint image where the fingerprint ridges

terminate/bifurcate or form an enclosure or island (lake) shape, and then match minutiae relative placements in a given finger and stored template as shown in Figure 1.6.

It is estimated that one can extract between 25 and 80 minutiae [6] from a good quality fingerprint. The number of minutia points extracted depends upon two factors: sensor resolution and finger placement on the sensor. It is well known that it is difficult to automatically and reliably extract minutiae points from a poor quality fingerprint due to very dry fingers or from fingers mutilated by scars as a result of accidents, injuries, or profession-related work (e.g., electrician, mason, and musician). Also, it was been observed that a fraction of the population fingers have a relatively small number of minutiae points which makes fingerprint-based identification more vulnerable to failures for such individuals.

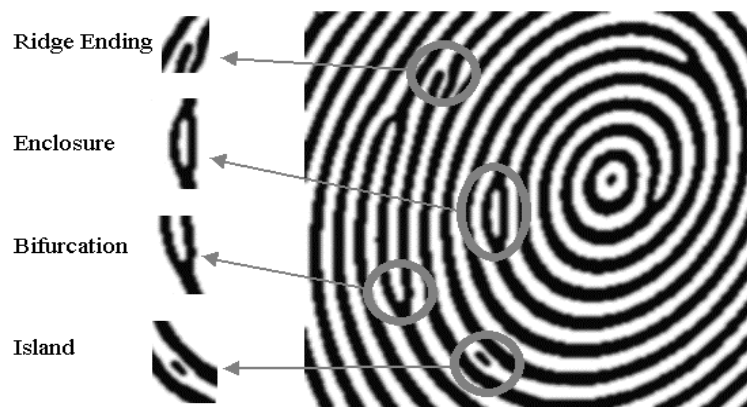


Figure 1.6: An illustration of minutiae points

1.3 Thesis Motivation

Most of the existing automatic fingerprint verification and classification systems use features that are motivated by the representations used by the forensic experts. Forensic experts have used the locations of singularities in the fingerprints (e.g., core & delta) to visually classify fingerprints for indexing purposes. Due to the increasing need for reliable individual automatic authorization and authentication systems, various biometric identification and verification systems have been developed, gaining a wide acceptance in law enforcement and civilian life applications such as access control. However, the performance of these systems is still far from the state-of-the-art theoretical bounds. This makes open room for new fingerprint matching algorithms/approaches. Existing fingerprint matching algorithms enjoy advantages and suffer from limitations.

One of these drawbacks is the limited information content of the minutiae representation. Therefore, non-minutiae based representations of fingerprints should be explored. In this thesis, a novel non-minutiae representation for fingerprints is proposed. The proposed representation is based on translation, rotation and scaling (TRS) invariants and affine moment invariants (AMIs) applied on the directional features of a fingerprint image. The objective of this work is to explore and investigate different approaches to advance and

improve the study of fingerprint biometrics, and boost the performance of existing fingerprint identification and verification systems.

1.4 Problem Statement

Fingerprint verification is the process of comparing test and enrolled skin ridge impressions from fingers to determine if the impressions are from the same finger. The nature of the fingerprint ridge skin proved that no two fingerprints are ever exactly alike. Most fingerprint matching algorithms are based on finding associations between two fingerprints, by detecting and comparing particular fingerprint features called minutia points. Although minutia-based algorithms usually provide good performance, they have problems matching fingerprints when only few minutiae points are successfully extracted. Texture- and transform-based matching methods have advantages dealing with such images as they utilize features which are not based solely on minutia templates. However, it should be noted that one main advantage of minutia-based approaches is that they are faster.

In this study, we introduce a new fingerprint matching algorithm based on TRS invariants and AMIs applied on the directional features of a fingerprint

image. The directional features are extracted by utilizing the directional filter bank (DFB) transform.

1.5 Outline of the Thesis

The rest of the thesis is organized as follows.

Chapter 2 provides an overview of various fingerprint representations, definitions and notations. Furthermore, it gives a general view of image segmentation, enhancement, and feature extraction techniques of fingerprint images along with a description of the main functionalities of fingerprint recognition systems. A discussion on wavelets, scale invariant feature operators, filter banks and directional filter banks will follow. The chapter concludes with an explanation of moments and moment invariants along with their categories, focusing on moment invariant to translation, rotation and scaling (TRS) and affine moment invariants (AMIs)

Related work in the area of fingerprint matching algorithms is presented in Chapter 3. Minutia-, correlation-, ridge-, and transform-based approaches are discussed therein in details. Chapter 4 gives a detailed description of the proposed fingerprint matching method. The technique of directional filter banks (DFBs) for extracting fingerprint directional components is explained.

Identifying the reference (core) point and establishing a region of interest (ROI) is illustrated. The proposed approach for applying moment invariant analysis, feature vector extraction and matching is detailed.

In Chapter 5, the experimental results are reported and discussed along with a detailed performance analysis. A performance comparison with the current state-of-the-art methods is carried out.

Finally, Chapter 6 gives a summary of the thesis work along with the contributions made in this thesis. The chapter concludes with an outline of some proposed research directions where the work described in this thesis can be further investigated.

CHAPTER 2

2. OVERVIEW OF FINGERPRINT-BASED BIOMETRIC SYSTEMS

2.1 Fingerprint Acquisition

There are two main modes of capturing a fingerprint. Traditionally, fingerprints were acquired by transferring the inked impression onto the paper. This process is termed as off-line acquisition. Existing authentication systems are based on live-scan devices that capture the fingerprint image using real-time sensors. There are different types of fingerprint readers in the market. Figure 2.1 shows examples of fingerprint scanners/readers based on different technologies. The basic idea behind each capture approach is to measure the physical differences between ridges and valleys. Generally speaking, existing scanners use sensors that employ one of the following three sensing schemes: optical, ultrasound, and solid-state sensors [5].



Figure 2.1: Fingerprint scanners/readers

Optical fingerprint imaging involves capturing a digital image of the print using a visible light. This type of sensor is, in essence, a specialized digital camera. This is the oldest and most widely used technology [1]. The top layer of the sensor, where the finger is placed, is known as the touch surface. Beneath this layer is a light-emitting device which illuminates the surface of the finger. The light reflected from the finger passes through to a charged coupled device (CCD) which captures a visual image of the fingerprint. These sensors are fairly inexpensive and can provide resolutions up to 500 dpi. Most optical sensors are based on FTIR (Frustrated Total Internal Reflection) technique to acquire the image [5].

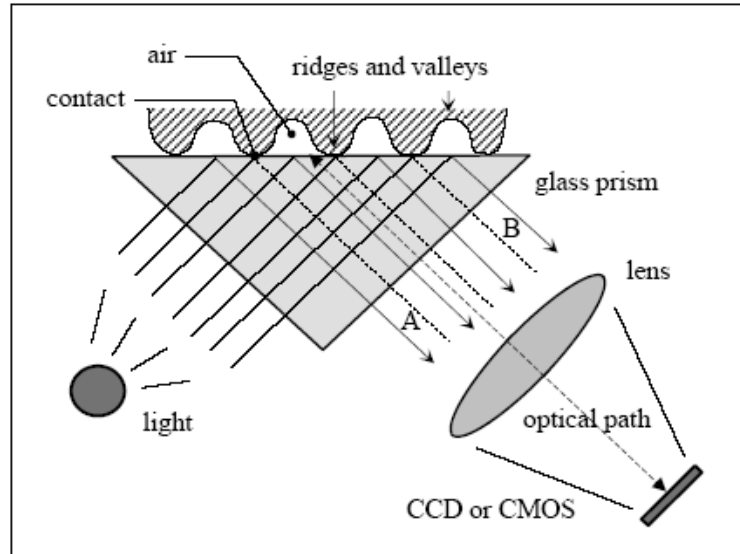


Figure 2.2: FTIR-based fingerprint sensor operation [5]

Ultrasonic sensors make use of the principles of medical ultrasonography in order to create visual images of the fingerprint. Unlike optical imaging, ultrasonic sensors use very high frequency sound waves to penetrate the epidermal layer of skin. Since the dermal skin layer exhibits the same characteristic pattern of the fingerprint, the reflected wave measurements can be used to form an image of the fingerprint. This eliminates the need for clean, undamaged epidermal skin and a clean sensing surface. However, these sensors tend to be very bulky and contain moving parts making them suitable only for law enforcement and access control applications [1].

Solid-state sensors also known as silicon sensors. The silicon sensor acts as one plate of a capacitor, and the finger itself as another capacitor. The

capacitance between the sensing plate and the finger depends inversely as the distance between them. Since the ridges are closer, they correspond to increased capacitance and the valleys corresponds to smaller capacitance. This variation is converted into an 8-bit gray scale digital image. Most of the electronic devices featuring fingerprint authentication use this form of solid state sensors due to its compactness.

2.2 System Functionalities

Figure 2.3 shows the functionalities of a fingerprint-based biometric system:

1. **Enrollment:** is the process of registering a new person to the system.
These steps can be summarized as follows: Scanning, feature extraction, and storing template in the database.
2. **Verification:** is the process of validating a person identity by matching his biometric trait with a template stored in the database.
The steps are as follows: Scanning, feature extraction, matching, and decision making.
3. **Identification:** is the process of searching all templates corresponding to users in the database for a match (one-to-many

comparisons). The steps have the sequence: Scanning, feature extraction, comparing with all templates, and decision making.

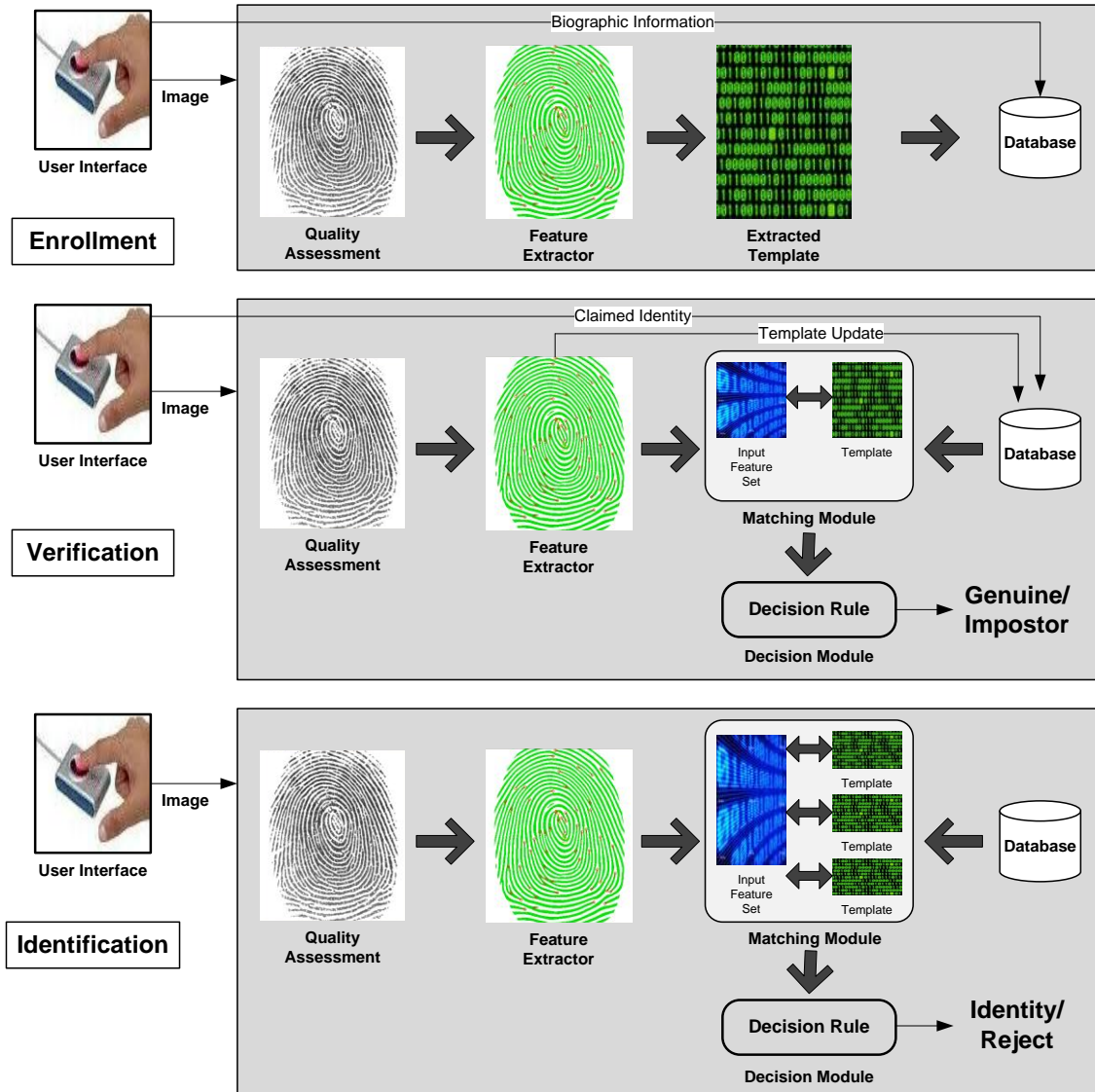


Figure 2.3: Fingerprint system functionalities.

2.3 Fingerprint Representation and Feature Extraction

There are two fingerprint representations, namely, local and global. The local representations in fingerprints are based on the entire image, finger ridges, pores on the ridges, or salient features derived from the ridges [7]. Representations are based mainly on ridge endings or bifurcations communally known as minutiae as shown in Figure 2.4.

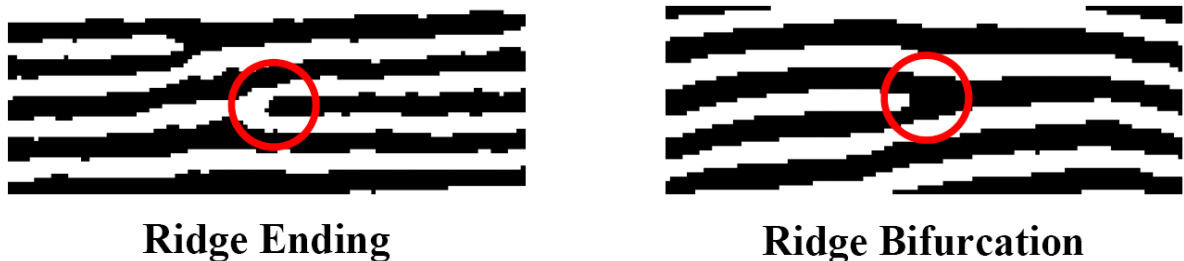


Figure 2.4: Ridge ending and ridge bifurcation.

Ridge endings and bifurcation are the most common due to their:

1. Ability to capture much of the individual information.
2. Storage efficiency.
3. Robustness to various sources of fingerprint degradation.

Typically, minutiae-based representations rely on locations and the directions of ridges at the minutiae location, i.e., described by its position (x,y) and its orientation θ [8].

Global representations include information about locations of critical points, namely, core(s) and delta(s), in a fingerprint to help classify a fingerprint into one of six classes arch, tented arch, right loop, left loop, whorl, and twin loop. The various fingerprint classes are illustrated in Figure 1.5.

To define core and delta, let us consider the Loop pattern as in Figure 2.5. A Loop is defined by having at least one ridge that enters the print and recurves back exiting the print on the same side. The top of the innermost recurving ridge is defined as the core.

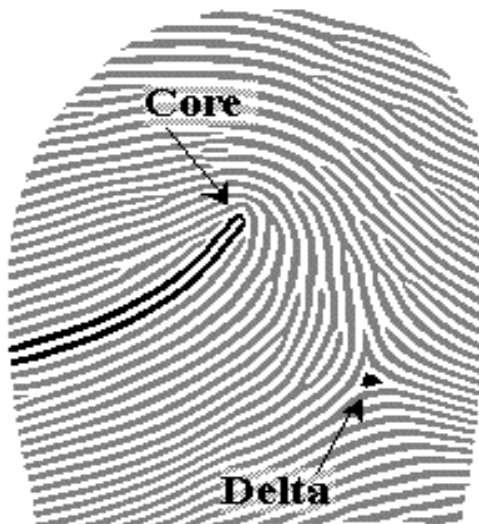


Figure 2.5: Core and delta.

The other side of a Loop contains ridges that enter the print and meet the recurving ridges. Some of these rise above, and some fall below the loop. The point where they diverge that is closest to the recurving ridges is the delta, (there is often a small island at this point).

However, extracting such features is not simply done through finding the ridge endings and ridge bifurcations. This process is heavily affected by the quality of the fingerprint image. In order to get reliable features, the extraction generally consists of the following steps [9]:

1. Orientation Estimation (which represents the directionality of ridges).
2. Segmentation.
3. Ridge detection.
4. Minutiae Detection.
5. Post-processing.

2.4 Fingerprint Preprocessing

2.4.1 Fingerprint Segmentation

Before extracting the features of a fingerprint, it is important to separate the fingerprint regions (presence of ridges) from the background. This limits the region to be processed and therefore reduces the processing time, storage

space and false (or low discriminate power) feature extraction. A correct segmentation may be, in some cases, very difficult, especially in poor quality fingerprint or noisy images. The same information used for feature extraction, such as contrast, ridge orientation and ridge frequency can be used for the segmentation. Also, segmentation can be done directly by considering as background the regions with quality below some threshold. Figure 2.6 shows the contour of the segmented region superimposed over the original image.

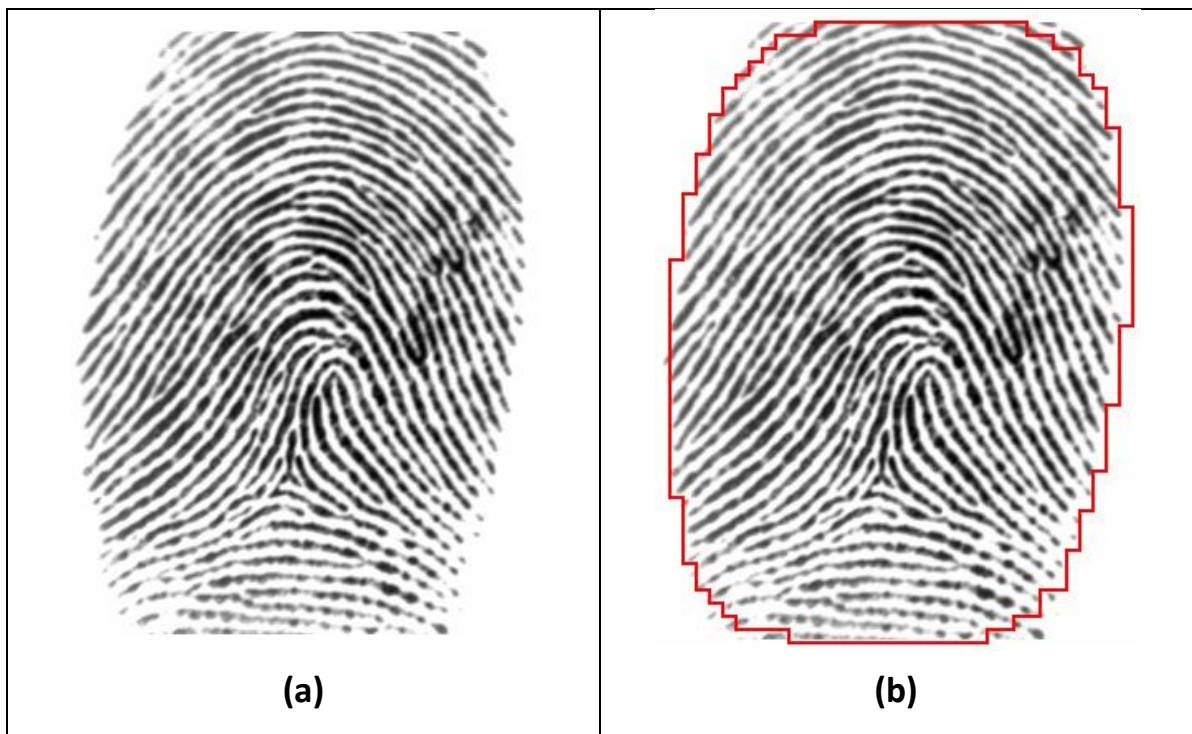


Figure 2.6: (a) original image (b) image with segmentation.

2.4.2 Fingerprint Enhancement

Enhancement step aims to improve the clarity of ridge structure or increase the consistence of the ridge orientation. In noisy regions, it is difficult to define a common orientation of the ridges. The enhancement may be useful for several cases like connecting broken ridges which is generally produced by dry fingerprint or cuts/bruises. Also, it is useful for eliminating noise between the ridges and improving the ridge contrast. There are two widely used techniques of enhancing fingerprint images [10]:

- **Normalization:** A simple method to improve the image quality by eliminating noise and correcting the deformations of the image intensity. The idea of normalization consists of changing the intensity of each pixel so that mean and variance of the whole image are changed to some predefined values.
- **Fast Fourier Transformation (FFT):** The Fourier transformation is widely used in digital signal and image processing. In particular, for detecting high or low frequencies. As the ridges have a structure of repeated and parallel lines, it is possible to determine the frequency and the ridge orientation using the FFT transform. Considering this characteristic, an image is divided into blocks of small sizes (e.g., 32x32). On each block, the FFT transform is applied and then

multiplied by its power spectrum raised to some value k (for instance 2), then the inverse FFT is applied on the resulting image. Figure 2.7 shows a fingerprint image and an enhanced image as a result of using FFT transform, which demonstrate the improvement in ridges contrast and connecting broken ridges.

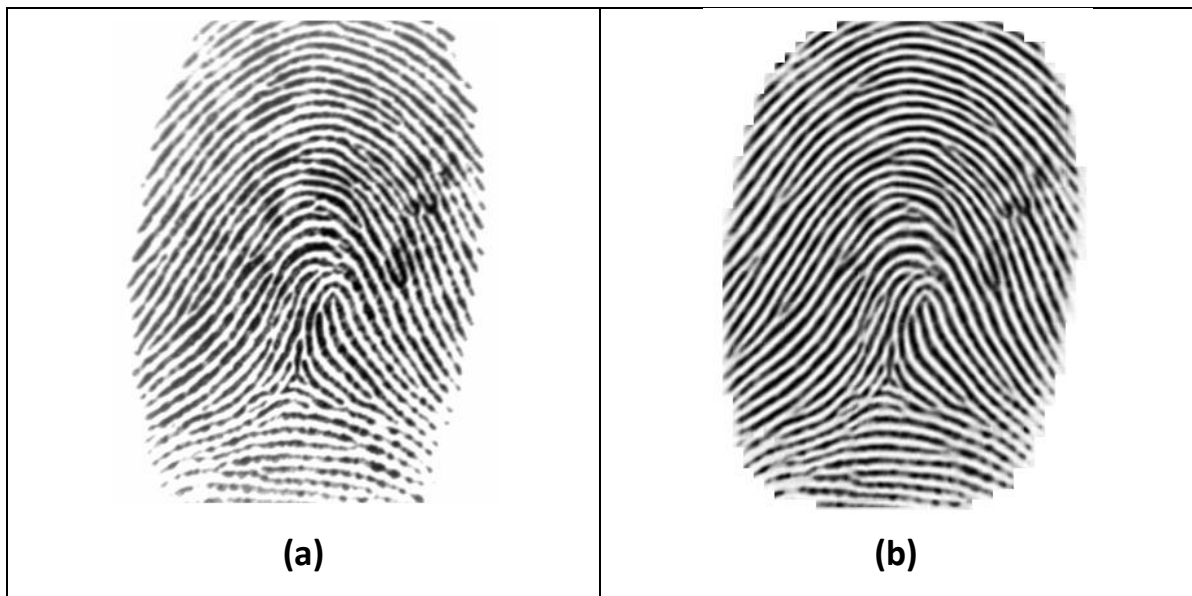


Figure 2.7: (a) original image (b) enhanced image using FFT.

2.4.3 Fingerprint Binarization/Skeletonization

The binarization process requires the fingerprint gray-scale image to be converted into a binary image. The simplest approach uses a global

threshold, th , and works by setting the pixels whose level is lower than th to 0 and the remaining pixels to 1. Then, the binary image is submitted to a thinning stage which allows for the ridge line thickness to be reduced to one pixel, resulting in a skeleton image. This process is illustrated in Figure 2.8.

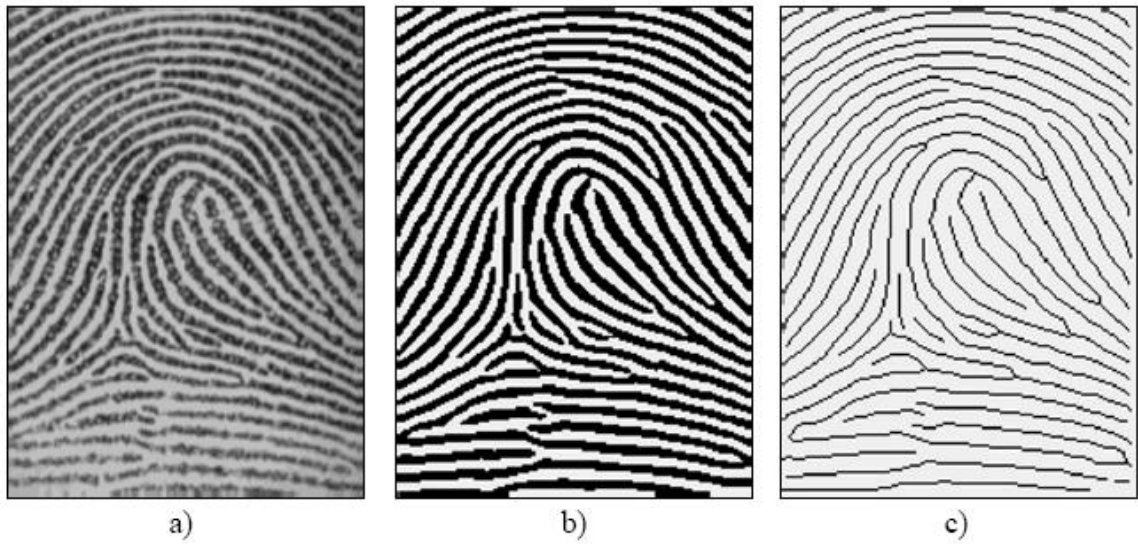


Figure 2.8: (a) gray-scale image (b) binarized image (c) skeleton image obtained after a thinning of the image in (b) [5].

2.5 Performance Measures

The performance of biometric systems is quantified by their accuracy. From the user's point of view, an error of accuracy occurs when the system fails to authenticate the identity of a registered person or when the system

erroneously authenticates an intruder. The following performance metrics are used in the evaluation of biometric systems:

- **False Accept Rate or False Match Rate (FAR or FMR):** The probability that the system incorrectly matches the input pattern to a non-matching template in the database. It measures the percent of invalid inputs which are incorrectly accepted.
- **False Reject Rate or False Non-Match Rate (FRR or FNMR):** The probability that the system fails to detect a match between the input pattern and a matching template in the database. It measures the percent of valid inputs which are incorrectly rejected.
- **Receiver Operating Characteristic (ROC):** The ROC curve is a visual characterization of the trade-off between the FAR and the FRR or the different possible thresholds. In general, the matching algorithm performs a decision based on a threshold which determines how close to a template the input needs to be for it to be considered a match. If the threshold is reduced, there will be less false non-matches but more false accepts. Correspondingly, a higher threshold will reduce the FAR but increases the FRR. A common variation is the Detection Error Trade-off (DET), which is obtained using normal deviate scales

on both axes. This more linear graph illuminates the differences for higher performances (rarer errors) [11].

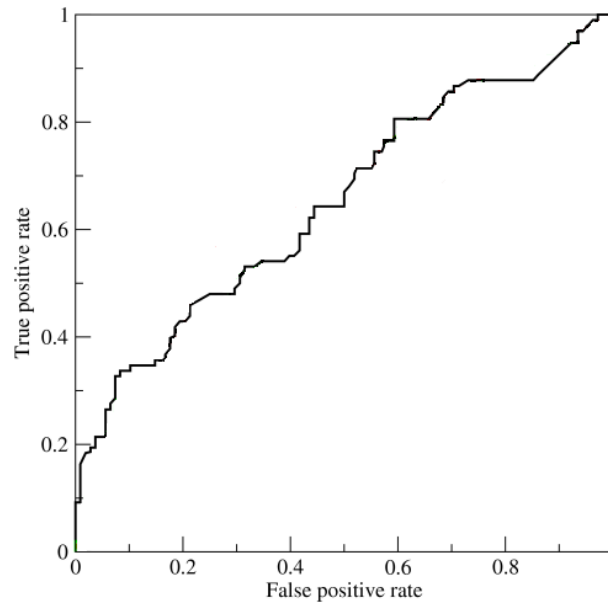


Figure 2.9: ROC curve is a plot of the true positive rate against the false positive rate for the different possible thresholds.

- **Equal Error Rate or Crossover Error Rate (EER or CER):** The rate at which both FAR and FRR errors are equal. The value of the EER can be easily obtained from the ROC curve. The EER is a quick way to compare the accuracy of systems with different ROC curves. In general, the system with the lowest EER is most accurate. The EER value is obtained from the ROC plot by taking the point where the

FAR and FRR have the same value ($FAR = FRR$) as Figure 2.10 shows.

The lower the EER, the more accurate the system is considered to be.

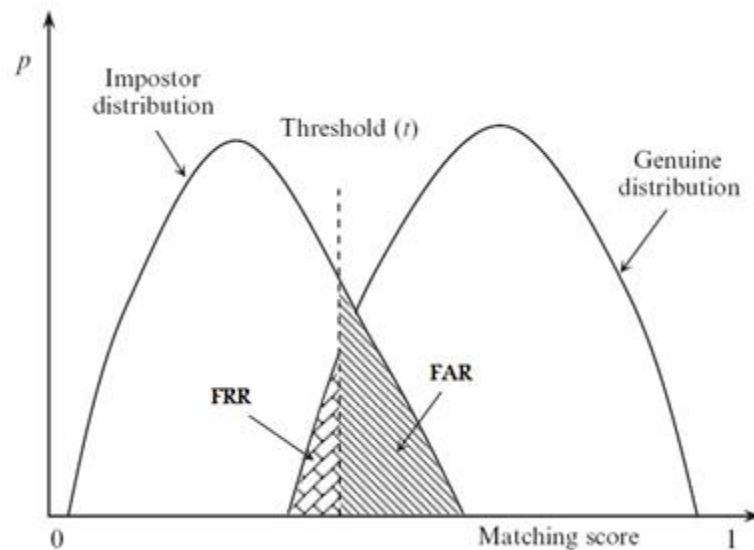


Figure 2.10: FAR and FRR for a given threshold (t), displayed over the genuine and impostor score distributions.

- **Failure to Enroll Rate (FTE or FER):** The rate at which attempts to create a template from an input are unsuccessful. This is most commonly caused by low quality inputs.
- **Failure to Capture Rate (FTC):** Within automated systems, the probability that the system fails to detect a biometric input when presented correctly.
- **Template Capacity:** The maximum number of sets of data which can be stored in the system.

2.6 *Benchmark Databases*

Due to the huge attention and research interest in the field of biometrics in general and fingerprint matching and classification in particular, various fingerprint databases have been constructed. It allows researchers to evaluate their proposed work against a benchmark, using the same conditions. Several databases are available for academic and research purposes.

The US National Institute of Standards and Technology (NIST) established a continuously updated fingerprint database to facilitate benchmarking for researchers in the law enforcement field. The NIST database consists of 2000 8-bit gray scale fingerprint images.

The International Fingerprint Verification Competition (FVC) uses a different set of fingerprint databases. There are 4 databases consisting of fingerprint images having different sizes and qualities. Figure 2.11 shows the typical images from the FVC databases.

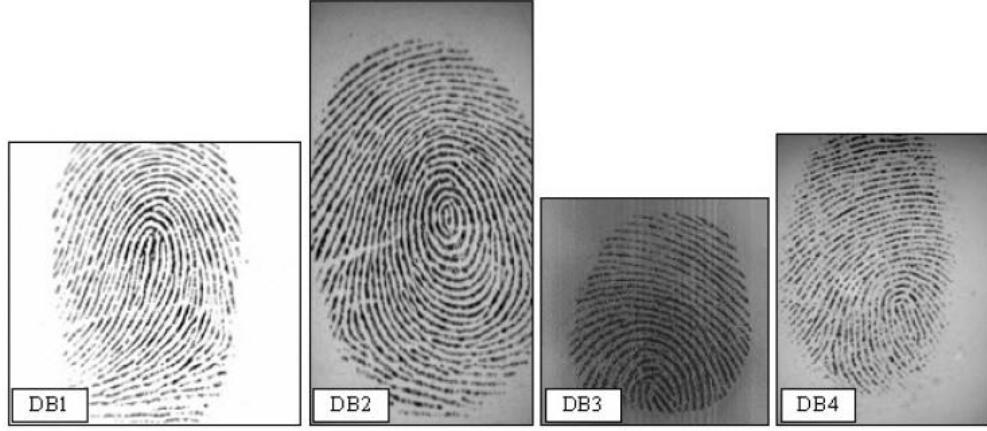


Figure 2.11: FVC2002 fingerprint database example [12].

Each database has 110 fingers and 8 impressions (samples) per finger (880 in total). Database fingers from 101 to 110 (set B) are available to the FVC participants before competition to allow parameter tuning before the submission of the algorithms. The benchmark is then constituted by fingers numbered from 1 to 100 (set A). Table 5.1 shows the basic components of the FVC2002 database.

	Sensor Type	Image Size	Set A	Set B	Resolution
DB1	Optical Sensor	388x374 (142 Kpixels)	100x8	10x8	500 dpi
DB2	Optical Sensor	296x560 (162 Kpixels)	100x8	10x8	569 dpi
DB3	Capacitive Sensor	300x300 (88 Kpixels)	100x8	10x8	500 dpi
DB4	SFinGe v2.51	288x384 (108 Kpixels)	100x8	10x8	about 500 dpi

Table 2.1: FVC2002 Fingerprint Database [12].

In this thesis, the FVC2002 database will be used for benchmarking purposes.

CHAPTER 3

3. RELATED WORK

3.1 Fingerprint Verification Methods

Fingerprint matching techniques can be cast into four broad classes, namely, minutiae, correlation, Ridge features (texture) and Transform based techniques. However, considering the types of information used, a method can be broadly categorized as minutiae based or texture based. While the minutiae based fingerprint verification systems have shown high accuracy [8, 11], they ignore the rich information in ridge patterns which can be useful to improve the matching accuracy.

Texture based systems utilize the whole fingerprint image and local features along minutiae points [13, 14]. This method is desirable because the global features will be more sensitive to non-linear and non-repeatable deformation of fingerprint images. When the local texture is collected based on the minutiae points, the texture based fingerprint representation will be

inadequate and matching performance will depend on the reliability of extracted minutiae points. Capturing the rich discriminatory texture information in the fingerprints is not a straight forward task, especially when such textures are not critically dependent on finding minutiae points [13] or core points [15].

3.1.1 Minutiae based Approach

As mentioned previously, minutiae points are defined as the discontinuities of the ridges of the fingerprint. Minutiae points are extracted after any image preprocessing (enhancement, segmentation etc.) to the fingerprint.

One of the proposed methods in the literature performs a minutiae verification and classification through a feedback path for the feature extraction [1]. Feng et al. [16] propose a technique for fingerprint feature extraction called *complex minutiae vector* (CMV). The technique consists of a ridge rotation angle associated with a minutia and four ridge counts between the minutia and the four corresponding adjacent points. In addition, a definition of minutia polygon that describes not only the minutia type and orientation but also the minutia shape, which has a higher ability to tolerate distortion [17].

3.1.2 Correlation based Approach

In [19], Duda and Hart investigate a technique, which relies on the correlation matching, uses correlation scores from the intensities of corresponding pixels of template and input fingerprint. Other researchers have proposed several improvements to the correlation method [20-22].

3.1.3 Ridge Features (Texture) based Approach

In [23], Marana and Jain present a texture-based fingerprint matching technique using fingerprint ridge features. Ross et al. [24] proposed a method to estimate the nonlinear distortion in fingerprint pairs based on ridge curve correspondences.

Filter banks and directional filter banks have attracted the attention of several researchers. Jain et al. [15] use a filter-based algorithm using bank of Gabor filters. Gabor filters are used to capture local and global details of a fingerprint into a fixed *FingerCode*. Then, performs the fingerprint matching using the Euclidean distance between the two corresponding FingerCodes.

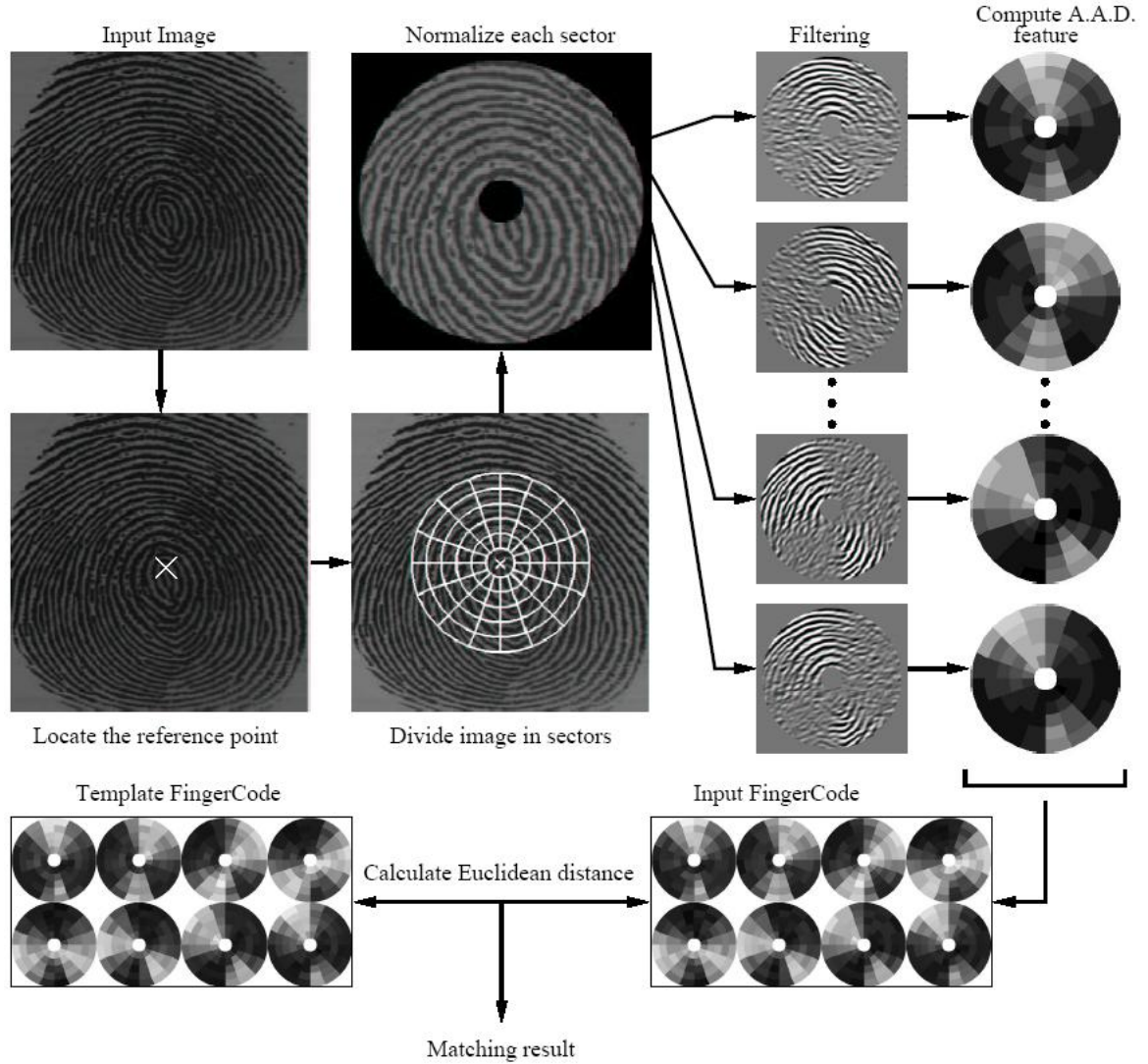


Figure 3.1: Texture Based matching Using a Filter-Bank of Gabor filters [15].

While, in [25], Oh et al. suggest a fingerprint enhancement (minimizing the effect of noise) algorithm based on a directional filter bank (DFB) by decomposing fingerprint image into directional sub-band images in the analysis stage, processes the sub-band images in the processing stage, and reconstructs them as the enhanced image in the synthesis stage. Park et al.

[26] proposed another approach based on DFB filtering. They decompose fingerprint image into eight directional sub-band outputs. Figure 3.2 illustrate the frequency decomposition of the input and output, along with an output example of a filtered image. Then, extract directional energy distributions for each block from the decomposed sub-bands. To reduce noise effect and improve efficiency, only dominant directional energy components are kept as elements of the input feature vector. Additional input feature vectors in which various rotations are considered are extracted, and these input feature vectors are compared with the enrolled template feature vector.

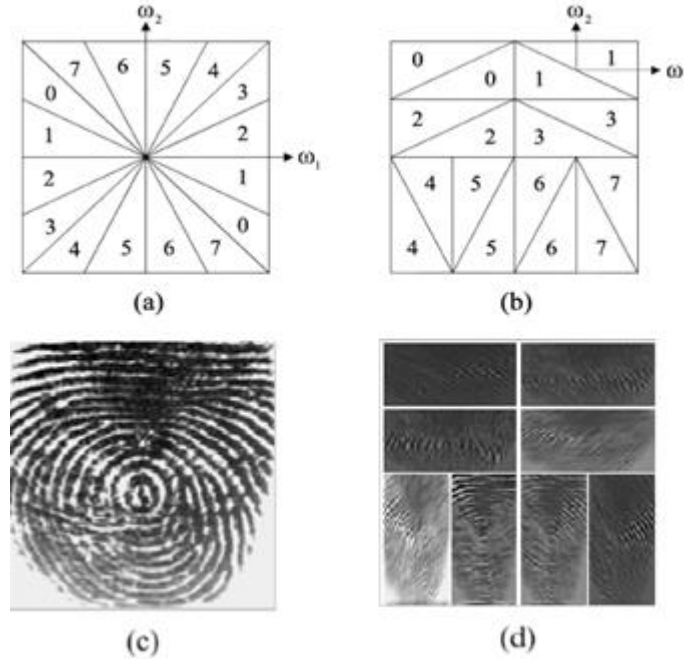


Figure 3.2: DFB illustration, Frequency partition map of (a) the input and (b) the eight sub-band outputs. (c) Example of fingerprint image. (d) Decomposed sub-band outputs of (c) using eight-band DFB.

3.1.4 Transform-Based based Approach

Transform based techniques have been used extensively in the literature. Park and Pankanti [6] proposed a fingerprint representation and matching scheme using Scale Invariant Feature Transformation (SIFT) (see Section 4.1 for details). It extract SIFT characteristic feature points in scale space and perform matching based on the texture information around the feature points using the SIFT operator and Euclidean distance to perform matching. In [28] Iannizzotto and La Rosa investigate combining SIFT with neural networks.

Also, a classification algorithm utilizing wavelet transform is investigated by Mokji and colleagues [29]. Fingerprint signatures are extracted by using the wavelet transform. Then, fingerprints are classified into six categories: 1) left loop, 2) right loop, 3) whorl, 4) arch 5) tented arch and 6) twin loop. After fingerprint image classification, a directional computation is used to present a directional image for the fingerprint image. The directional image is constructed using directional details resulting from the application of the wavelet transform. From the directional image, a line, named *alteration track*, is extracted in order to classify the fingerprint using few rules. Lee and Chung [30] utilized gradient of Gaussian to do the classification after

extracting the features using wavelet. Antonini et al. [31] devised and tested an image coding technique, based on the wavelet transform.

Moreover, Mokji and others, used a second stage discrete wavelet transform to obtain the fingerprint signature to be used by the fingerprint classification algorithm [32]. Patil and others [34], proposed a combined fingerprint verification approach based on wavelet transform and the local dominant orientation. Daubechies wavelet is utilized to decompose the fingerprint image, and local dominant orientation is computed using the coherence.

CHAPTER 4

4. MATHEMATICAL BACKGROUND

4.1 *Scale Invariant Feature Transform SIFT*

Scale Invariant Feature Transformation (SIFT) [14] is an algorithm in computer vision to detect and describe local features in images. The algorithm was published by David Lowe in 1999. It was originally developed for general purpose object recognition. For any object in an image, there are many features which are interesting points on the object, that can be extracted to provide a feature description of the object. This description extracted from a training image can then be used to identify the object when attempting to locate the object in a test image containing many other objects [35]. It is important that the set of features extracted from the training image is robust to changes in image scale, noise, illumination and local geometric distortion, for performing reliable recognition. SIFT detects stable feature points in an image and performs matching based on the

descriptor representing each feature point. SIFT feature descriptor is invariant to scale, orientation, affine distortion and partially invariant to illumination changes [36]. A brief description of the SIFT operator to fingerprints is provided below.

Stage1: Scale Space Construction

This is the stage where the interest points are detected. A scale space is constructed when image is convolved with Gaussian filters at different scales, and then the Difference of Gaussian (DOG) in each octave of successive Gaussian-blurred images are taken by applying a variable scale Gaussian operator on an input image. The set of Gaussian-smoothed images and DOG images are called an octave. A set of such octaves is constructed by down sampling the original image in succession. A typical number of scales and octaves for SIFT operation is 5 and 6, respectively. Figure 5 shows 4 successive octaves with 5 scales and the corresponding difference images.

Stage2: Local Extrema

Once DoG images have been obtained, keypoints are identified as local minima/maxima of the DoG images across scales. This is done by comparing each pixel in the DoG images to its eight neighbors at the same scale and

nine corresponding neighboring pixels in each of the neighboring scales. If the pixel value is the maximum or minimum among all compared pixels, it is selected as a candidate keypoint.

Stage3: Stable Local Extrema and Orientation assignment

Keypoints detected using Scale-space extrema detection are too many, some of which are unstable. The next step is to perform a detailed fit to the nearby data for accurate location, scale, and ratio of principal curvatures. For More detailed description of this process can be found in the original paper by Lowe [36]. If an extremum is decided as unstable, it is removed because it cannot be reliably detected again with small variation of viewpoint or lighting changes. After that, each keypoint is assigned one or more orientations based on local image gradient directions.

Stage: Assigning Descriptor

After extracting keypoint locations at particular scales and assigned orientations to them, a 16x16 window [30] is used to generate a histogram of gradient orientation around each local extremum and rotate all gradient with respect to the major orientation of the local extremum. This ensures invariance to image location, scale and rotation.

- Example Figure

Matching is performed by comparing each local extrema based on the associated descriptors. Figure 4.1 illustrates the steps of scale space construction for SIFT operator.

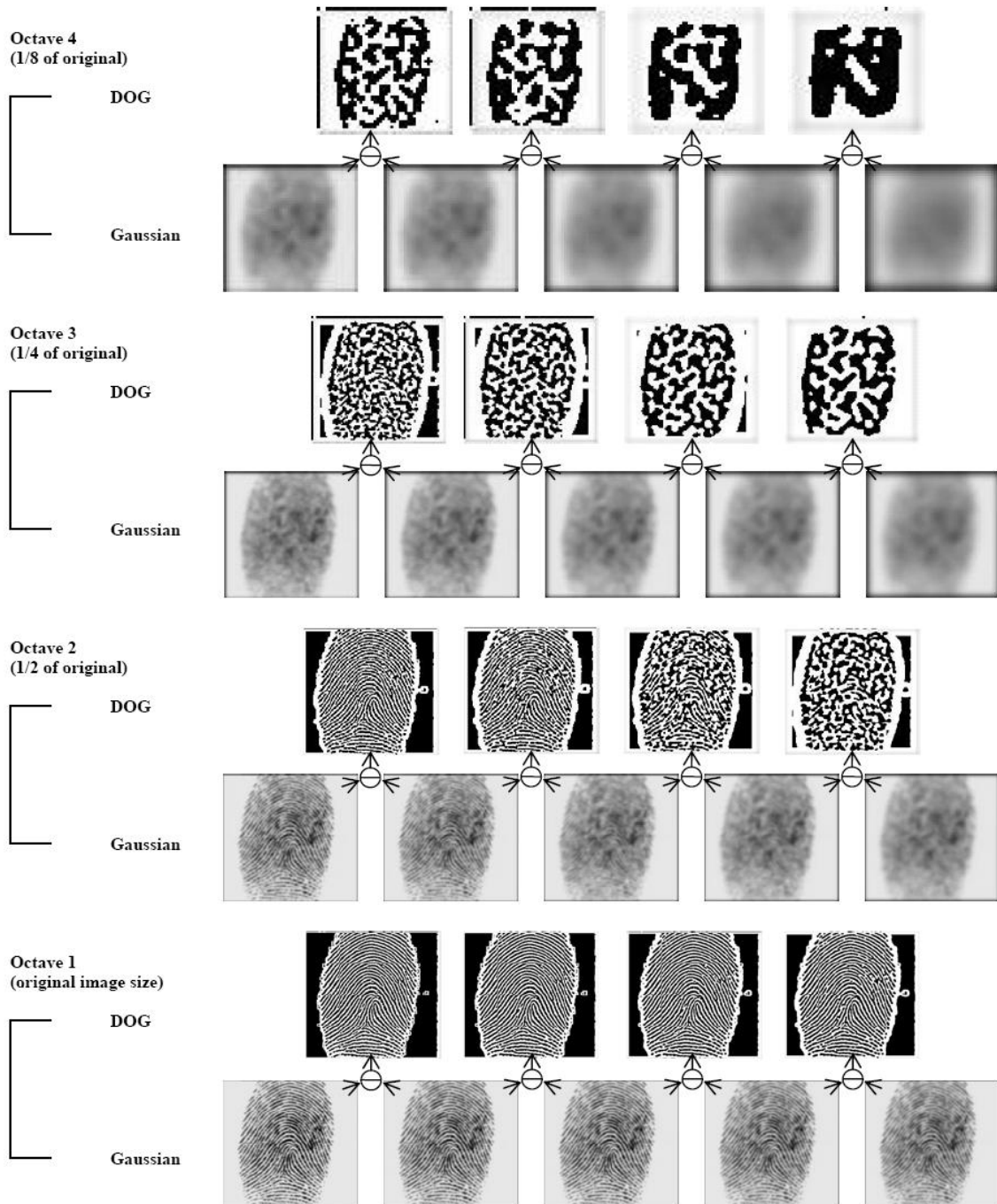


Figure 4.1: Scale space construction for SIFT operation [6].

4.2 Discrete Wavelets

A wavelet is a waveform of limited duration that has an average value of zero. Unlike sinusoids that theoretically extend from minus to plus infinity, wavelets have a beginning and an end, as shown in Figure 4. 2.

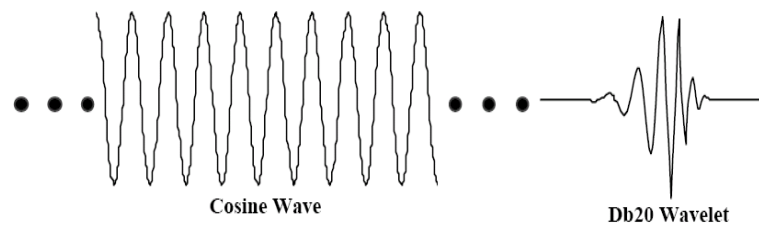


Figure 4.2: Difference between cosine wave and wavelet.

Mathematically speaking, Wavelets are defined by the wavelet function $\psi(t)$ (i.e. the mother wavelet) and scaling function $\phi(t)$ (also called father wavelet) in the time domain. The wavelet function is in effect a band-pass filter and scaling it for each level halves its bandwidth. This creates the problem that in order to cover the entire spectrum, an infinite number of levels would be required. The scaling function filters the lowest level of the transform and ensures all the spectrum is covered [37].

Wavelets are a useful technique that can be applied to many tasks in signal processing. First, we need to Locate core point and crop fingerprint image

around core point. Then, a modified version of Daubechies' wavelet can be applied to a fingerprint image to get the directional characteristics as shown in Figure 4. 3.

Since directional information obtained from wavelets does not represent all directions, we cannot use them directly. To overcome this issue and construct a feature vector that capture more detailed directional information a gradient of Gaussian and coherence is applied to the wavelet [27].

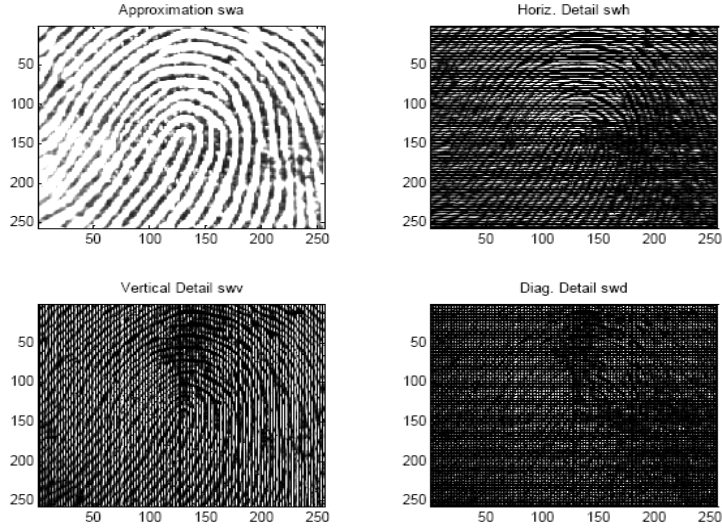


Figure 4.3: Wavelet Decomposed Fingerprint.

Gradient G_{mn} , and corresponding angle θ_{mn} at the position (m, n) are defined as:

$$G_{mn} = M \times (|G_{mn}^x| + |G_{mn}^y|) \quad (1)$$

$$\theta_{mn} = \tan^{-1} \left[G_{mn}^y / G_{mn}^x \right] \quad (2)$$

After estimating the G_{mn} and θ_{mn} , we estimate local dominant orientation using coherence ρ_{mn} , which is defined as:

$$\rho_{mn} = \frac{\sum_{(i,j) \in w} G_{ij} \cos(\theta_{mn} - \theta_{ij})}{\sum_{(i,j) \in w} G_{ij}} \quad (3)$$

The coherence images with size of window w (5x5) are shown in Figure 4.4. After that, the dominant local orientation is calculated from the gradient and coherence. The dominant local orientation θ is defined as:

$$\theta = \frac{1}{2} \tan^{-1} \left[\frac{\sum_{m=1}^M \sum_{n=1}^N \rho_{mn}^2 \sin(2\theta_{mn})}{\sum_{m=1}^M \sum_{n=1}^N \rho_{mn}^2 \cos(2\theta_{mn})} \right] + \pi/2 \quad (4)$$

where M and N are equal to 8, to represent one directional information per 8x8 window. Finally, the variance and energy of each block are computed.

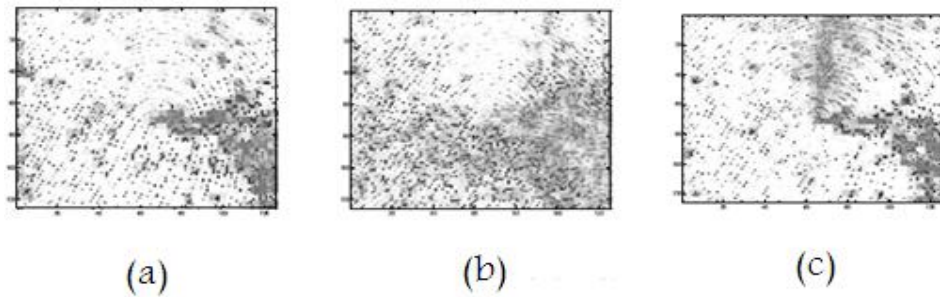


Figure 4.4: Coherence images: (a) Approximate image, (b, c) Horizontal, Vertical details.

4.3 Directional Wavelets and Filters

Wavelet transform to an image results in four domains contain directional image that are horizontal, vertical and diagonal. Wavelet transform comes with many types [38] (Haar, Shannon, Meyer, Daubechies, and Coifmann wavelets) and can be done in multilevel decomposition. The wavelet transform is identical to a hierarchical sub band system where the sub- bands are logarithmically spaced in frequency and represent octaveband decomposition [31]. Wavelets provide rich techniques that can be applied to many tasks in signal processing, and therefore have numerous potential applications [30].

There are three steps to construct the directional image [29]. First, we need to transform the original image using wavelet transform. Secondly, the output from the wavelet transform is used to construct the directional image. Finally, the directional image is smoothed to get better directional image.

So, wavelets are defined by a mathematical expression and are drawn as continuous and infinite, which are called “crude wavelets”. However, to use them with our digital signal, they must first be converted to wavelet filters having a finite number of discrete points. That is, we evaluate wavelet equation at the points of time that interest us in order to create filter values at

those times [38]. Conversely, some wavelets start as filters with as little as 2 points and built up by interpolating and extrapolating more points to get an estimation of a continuous wavelet.

4.4 *Filter Banks*

The main concern when we want to obtain a representation for fingerprints is to be invariant to scale, translation and rotation. Scale invariance is not a big issue since this can be handled by scaling the fingerprint per dpi. The rotation and translation has another story since it does not follow the assumption that the fingerprints are vertically oriented, which most of the feature extraction implementation do assume [15]. Most fingerprint databases may have fingerprints that are oriented by up to $\pm 45^\circ$ away from the assumed vertical orientation.

The problem with rotation could be handled, to some degree, with cyclic rotation of the feature values, while the translation is addressed by establishing a one reference point location during the feature extraction and using a bank of Gabor filters on the region of interest around the reference point, as shown in Figure 4.5. This will show enhancement of the ridge structures using both one local ridge direction and local frequency information as inputs for filtering.



Figure 4.5: Reference point (X), and region of interest divided into 80 sectors imposed on the fingerprint.

A directional filter bank (DFB) analyzes an input image into directional sub-band images and synthesizes them to the perfectly reconstructed image. The DFB decomposes a fingerprint image into many directional sub-band images and reconstruct the enhanced output image by synthesizing the filtered outputs, which are blocks with the greatest energy among the sub band images. DFB realizes a division of 2-D spectrum into 2^n wedge-shaped slices as shown in Figure 4.6, using an n-levels iterated tree structured filter banks.

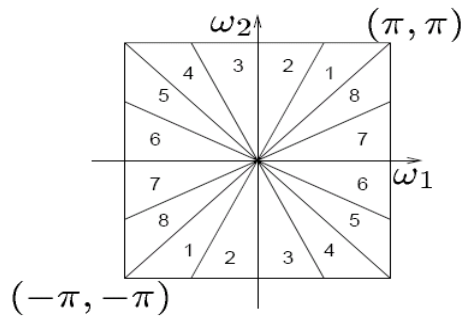


Figure 4.6: Directional filter bank frequency partitioning [39].

The energy for each sub-band image is used to estimate the direction of each block in the original image. The directional energy of block (I, J) including the pixel (i, j) from the k^{th} sub-band image is defined as:

$$E_k(I, J) = \sum_{i=0}^{m_k} \sum_{j=0}^{n_k} |f_k(I, J; i, j)| \quad (5)$$

The direction of each block for a directional image is generated based on the direction corresponding to the sub-band with maximum energy among all bands at each block. The direction of a block in a fingerprint is calculated by using gradient-based methods, in which a gradient operator or eight one-dimensional masks in eight directions are used [39].

Because the gradient operator uses a derivative operation, the results are sensitive to noise. This can be avoided by taking the direction corresponding to the largest information content in a block so the result will be more robust to noise. So, the direction of a block is defined by:

$$d(I, J) = m, \text{ if } \underset{m}{\text{Maximize}}[E_m(I, J)] \quad (6)$$

To insure that an injured ridge does not affect the ridge direction, a process of directional averaging [40] could be done and its block direction should be defined as $\bar{d}(I, J)$. The resulting directional image overlapping with the original image is shown in Figure 4.7.

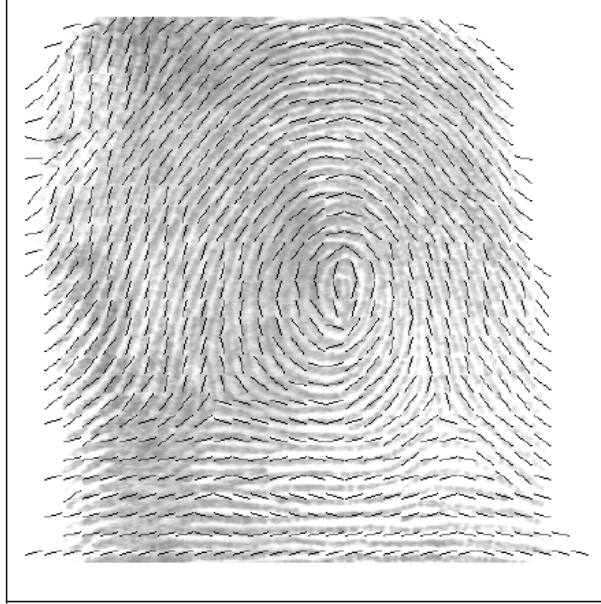


Figure 4.7: Directional image [25].

5.5 Directional Filter Bank

In order to make this thesis practically self contained, we provide a brief description of the DFB architecture employed in this work. The description is sufficient to provide insight into how the DFB works but without the details of implementation. The original concept of the DFB was introduced by Bamberger and Smith [40] and later refined by Park et al. [44]. The

interested reader is referred to those two papers for additional detail. The DFB divides the two-dimensional (2-D) spectrum of an image into wedge-like directional sub-bands, as shown in Figure 4.8 (a). Eight directional sub-band outputs can be obtained using the DFB, as shown in Figure 4.8 (b). Figures 3.2(c,d) shows an example of the directional sub-band images decomposed by the eight-band DFB, where each directional component is captured in its own sub-band image. The DFB basically consists of lowpass filters (\mathbf{H}_0), quincunx down samplers (\mathbf{Q}), diamond conversion matrices (\mathbf{R}), modulators ($e^{-j\omega_1 \pi}$), and postsampling matrices (\mathbf{B}), as shown in Figure 4.1. The modulator varies the spectrum of the image so that the modulated image can be divided into two directional sub-band images by a lowpass filter with a diamond-shaped pass-band. Meanwhile, the quincunx down sampler simultaneously down samples the image and rotates it by 45 degrees.

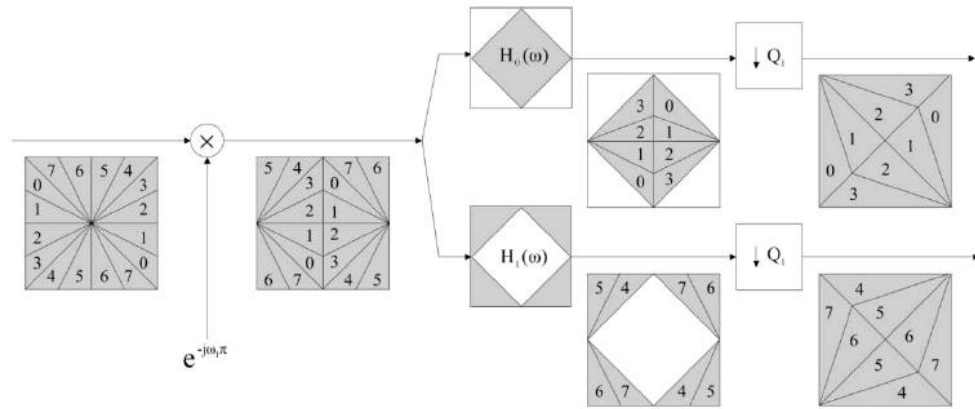


Figure 4.8: First phase of an eight-band DFB.

As shown in Figure 4.8, the input is modulated, filtered, and downsampled, resulting in two sub-band images. Then the two sub-band images are further divided into four sub-band images using a procedure similar to that used in the first step, as illustrated in Figure 4.9. At final phase, diamond conversion matrices are required to transform the parallelogram-shaped pass-band into one with a diamond shape. These diamond conversion matrices enable the DFB to be implemented using only a one-dimensional (1-D) filter prototype.

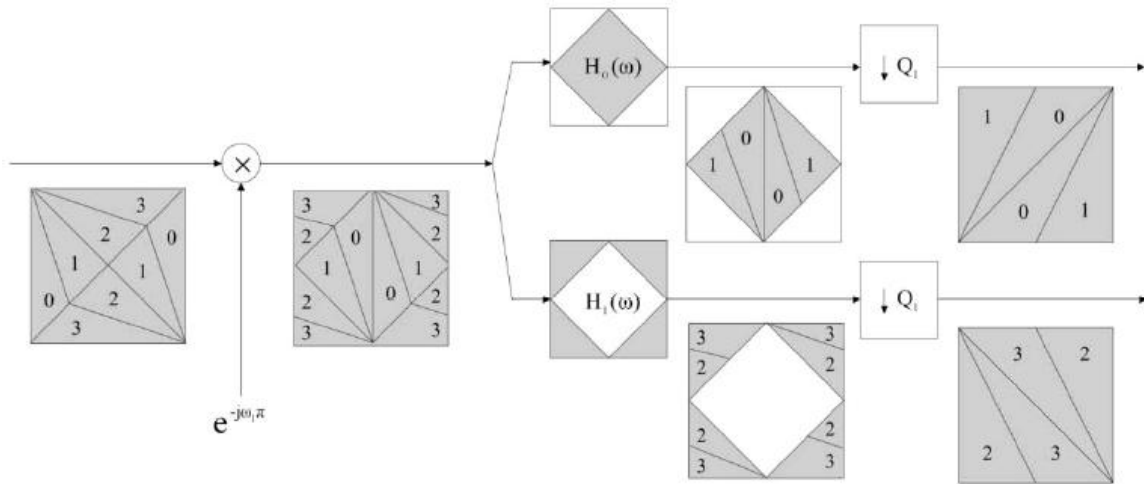


Figure 4.9: Second phase of an eight-band DFB.

Postsampling matrices are then appended to the end of the filter bank to remove the phenomenon of frequency scrambling, resulting from the frequency shift due to the modulator and nondiagonality of the overall down sampling matrix. Filter bank stages can be implemented in a separable polyphase form to achieve highly efficient realizations. Then, an eight directional sub-band outputs are generated as in Figure 4.10.

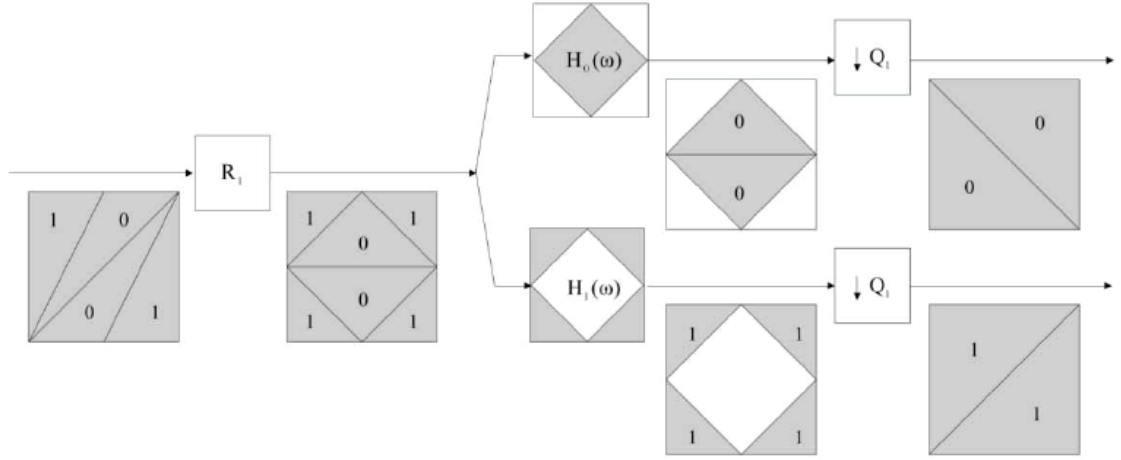


Figure 4.10: Third phase of an eight-band DFB.

In this thesis, we propose the use of the DFB structure, defined in [40], where the design of the lowpass filters is achieved through a linear phase IIR filter. As a result of the downsampling, the eight-band decompositions are rectangular. The analysis stage is based on a third-order decomposition of $N \times N$ images leading to eight sub-bands where the first half of the sub-bands

has a size of $N/4 \times N/2$, while the other half has a size of $N/2 \times N/4$, respectively.

4.6 Curvelets

The curvelet transform is obtained by filtering and then applying windowed ridgelet transform on each bandpass image. This is done by Sub-band decomposition of the object into a sequences of sub-bands. After that, each sub-band is windowed into blocks of appropriate size, depending on its center frequency. Finally, ridgelet transform will be applied on windowed blocks [41]. Therefore, curvelet, as shown in Figure 4.11, basis functions can be viewed as a local grouping of wavelet basis functions into linear structures so that they can capture the smooth discontinuity curve more efficiently [42].

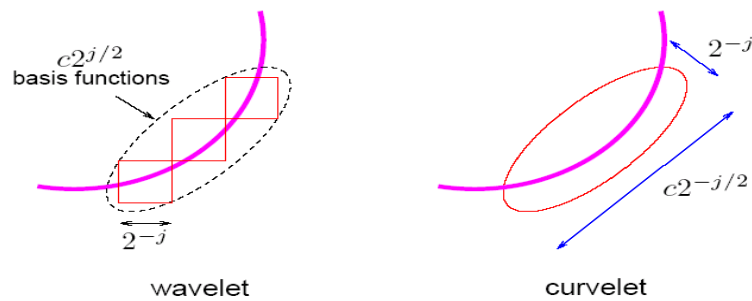


Figure 4.11: Wavelet vs. Curvelet [42].

4.7 *Invariants*

Recognizing patterns in images has three main approaches: brute force, image normalization and invariant features. The brute force require the use of all possible representation of images which include their rotated, scaled, blurred and deformed versions [43]. This method will have a very high time complexity which is not applicable.

The normalization approach transforms the image into a standard position which requires the solving of difficult inverse problems that are ill-posed or ill-conditioned.

The invariants approach uses a set of measurable quantities that are insensitive to particular deformation. Those invariants features have enough discriminating power to distinguish patterns into different classes. Mathematically speaking, selected features have the property called invariance which can be expressed as:

$$I(f) = I(D(f)) \quad (7)$$

That is invariant I is a function that does not change its value under degradation operator D .

4.7.1 Categories of Invariants

Invariants have different categories based on different points of view. There are four ways to categorize invariants:

- Based on the type of invariance, namely, translation, rotation, scaling, affine, projective, and elastic geometric invariants.
- Radiometric invariants exist with respect to linear contrast stretching, nonlinear intensity transformers, and convolution.
- Categorization based on the mathematical tools used like:
 - Simple shape descriptor – like compactness, convexity, elongation, etc.
 - Transform coefficient features – like Fourier, wavelet, and Hadamard descriptors.
 - Point set invariants – which uses positions of dominant points.
 - Differential invariants – which uses derivatives of the object boundary.
 - Moment invariants – which uses special functions of image moments.
- Categorization based on the part of the object needed to calculate the invariant:

- Global invariants – which is calculated from the whole image.
- Local invariants – which is calculated from dominant points.
- Semilocal invariants – which uses properties from both global and local invariants.

4.8 Moments

Moments are scalar quantities used to characterize a function and to capture its significant features, which is used in statistics for describing the shape of a probability density function [43]. Mathematically speaking, moments are “projections” of a function onto a polynomial basis.

Broadly speaking, Moments are categorized according to the polynomial basis used into geometric & complex moments, and orthogonal moments. In image processing field, a moment is a certain particular weighted average of the image pixels intensities, or a function of such moments, usually chosen to have some attractive property or interpretation. Image moments are useful to describe objects after segmentation. Simple properties of the image which are found via image moments include area, intensity, centroid, and information about its orientation.

The geometric moments of 2-D continuous function $f(x,y)$, with a standard power basis $k_{pq}(x, y) = x^p y^q$ is defined by:

$$M_{pq} = \int_{-\infty}^{\infty} \int_{-\infty}^{\infty} x^p y^q f(x, y) dx dy \quad (8)$$

for $p, q = 0, 1, 2, \dots, n$

Adapting the above equation to scalar (grayscale) image with pixel intensities $I(x, y)$, raw image moments M_{ij} are calculated by:

$$M_{ij} = \sum_x \sum_y x^i y^j I(x, y) \quad (9)$$

Complex moments are based on the polynomial basis $k_{pq}(x, y) = (x + iy)^p (x - iy)^q$ is defined by:

$$c_{pq} = \int_{-\infty}^{\infty} \int_{-\infty}^{\infty} (x + iy)^p (x - iy)^q f(x, y) dx dy \quad (10)$$

Orthogonal (OG) moments are preferred in the literature because they are fast and stable numerical implementation [43]. Another reason why OG moments are used is due to better image construction. A 2D polynomial orthogonal on a rectangle is constructed as products of 1D OG polynomials $p_k(x)$. The OG moments will have the form:

$$v_{pq} = n_p n_q \iint_{\Omega} p_p(x) p_q(y) f(x, y) dx dy \quad (11)$$

Where n_p, n_q are some normalized factors and Ω is the area of orthogonality.

The image $f(x, y)$ should be scaled such that its support is contained in Ω .

As an illustration we took an image and rotated 5°, and 10°, respectively as shown in Figure 4.12.

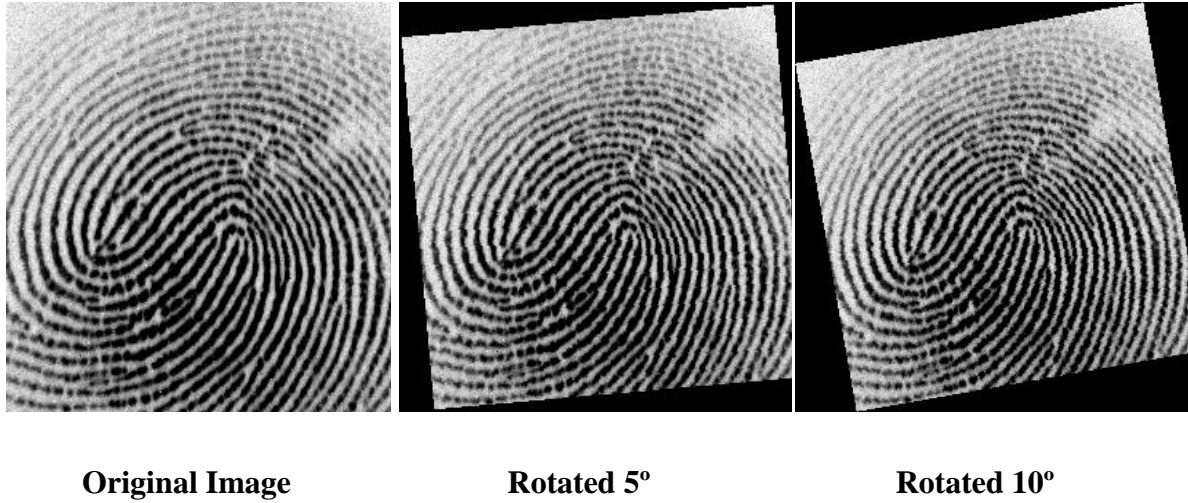


Figure 4.12: Rotated fingerprint example.

The Hu moments and Rotation invariants are presented in Table 4.1.

	1 st Hu Moments		Rotation Invariant
Original Image	$\Phi_1 = 0.3561$	$\Phi_5 = 0.0000$	6.7343
	$\Phi_2 = 0.0007$	$\Phi_6 = -0.0000$	18.6358
	$\Phi_3 = 0.0002$	$\Phi_7 = -0.0000$	25.7912
	$\Phi_4 = 0.0009$		24.8585
Rotated 5°	$\Phi_1 = 0.3563$	$\Phi_5 = 0.0000$	51.6173
	$\Phi_2 = 0.0007$	$\Phi_6 = -0.0000$	6.7345
	$\Phi_3 = 0.0002$	$\Phi_7 = -0.0000$	18.6301
	$\Phi_4 = 0.0009$		25.7919
Rotated 10°	$\Phi_1 = 0.3561$	$\Phi_5 = 0.0000$	24.8507
	$\Phi_2 = 0.0007$	$\Phi_6 = -0.0000$	51.3166
	$\Phi_3 = 0.0002$	$\Phi_7 = -0.0000$	6.7344
	$\Phi_4 = 0.0009$		18.6332

Table 4.1: Hu moments & Rotation Invariants.

4.9 *Moment Invariants to Translation, Rotation and Scaling*

Moment features can provide the properties of invariance to scale, position, and rotation [43]. This section gives a brief description of the moment analysis.

For a 2-D continuous function $f(x, y)$, the moment of order $(p + q)$ is defined as:

$$m_{pq} = \int_{-\infty}^{\infty} \int_{-\infty}^{\infty} x^p y^q f(x, y) dx dy \quad (12)$$

for $p, q = 0, 1, 2, \dots$

The central moments are defined as:

$$\mu_{pq} = \int_{-\infty}^{\infty} \int_{-\infty}^{\infty} (x - x_c)^p (y - y_c)^q f(x, y) dx dy \quad (13)$$

Where,

$$x_c = \frac{m_{10}}{m_{00}} \quad \text{and} \quad y_c = \frac{m_{01}}{m_{00}} \quad (14)$$

If $f(x, y)$ is a digital image, then (13) becomes:

$$\mu_{pq} = \sum_x \sum_y (x - x_c)^p (y - y_c)^q f(x, y) \quad (15)$$

Invariance is obtained by proper normalization of each moment. In principle, any moment can be used as a normalizing factor provided that it is nonzero for all images in the experiment. Since low-order moments are more stable to

noise and easier to calculate, we normalize most often by a proper power of μ_{00} as follows:

$$v_{pq} = \frac{\mu_{pq}}{\mu_{00}^w} \quad (16)$$

Where,

$$w = \frac{p+q}{2} + 1 \quad (17)$$

The moment v_{pq} is called normalized central geometric moment. Note that the moment that was used for scaling normalization can no longer be used for recognition because the value of the corresponding normalized moment is always one.

4.10 Affine Moment Invariants

Affine moment invariants (AMIs) play a very important role in moment-based pattern recognition applications. They are invariant with respect to affine transform of the spatial coordinates. Affine transformation is a general linear transform of spatial coordinates of the image, which can approximate the projective transform [43].

The theory of AMIs is closely connected to the theory of algebraic invariants and the Fundamental theorem describes this connection. The algebraic invariant is a polynomial of coefficients of a binary form, whose value

remains the same after an affine transform of the coordinates. In the theory of algebraic invariants, only the transforms without translation are considered.

Let us consider an image f and two arbitrary points (x_1, y_1) , (x_2, y_2) from its support. Let us denote the “cross-product” of these points as C_{12} :

$$C_{12} = x_1 y_2 - x_2 y_1 \quad (18)$$

After an affine transform, it holds that:

$$C_{12} = J \cdot C_{12} \quad (19)$$

Which means that C_{12} is a relative affine invariant. We consider various numbers of points and we integrate their cross-products on the support of f . These integrals can be expressed in terms of moments and, after proper normalization, they yield affine invariants.

Mathematically, having r points ($r \geq 2$) we define functional I depending on r and on non-negative integers n_{kj} as:

$$I(f) = \int_{-\infty}^{\infty} \int_{-\infty}^{\infty} \prod_{k,j=1}^r C_{kj}^{n_{kj}} \cdot \prod_{i=1}^r f(x_i, y_i) dx_i dy_i \quad (20)$$

Note that it is meaningful to consider only $j > k$, because $C_{kj} = -C_{jk}$ and $C_{kk} = 0$. After an affine transform, $I(f)$ becomes:

$$I(f)' = J^w |J|^r \cdot I(f) \quad (21)$$

where $w = \sum_{k,j} n_{kj}$ is called the weight of the invariant and r is called the degree of the invariant. If $I(f)$ is normalized by μ_{00}^{w+r} , we obtain a desirable absolute affine invariant:

$$\left(\frac{I(f)}{\mu_{00}^{w+r}} \right)' = \left(\frac{I(f)}{\mu_{00}^{w+r}} \right) \quad (22)$$

The maximum order of moments of which the invariant is composed is called the order of the invariant. The order is always less than or equal to the weight.

An important note here is that we can generate as many invariants as we wish but only a few of them are independent. Since dependent invariants are useless in practice, in a sense that it does not increase the discrimination power of the recognition system at all while increasing the dimensionality of the problem. This leads to growth of the complexity and even to misclassifications.

4.10.1 Dependencies Among the AMIs

There might be various kinds of dependency in the set of all AMIs. They can be categorized into five groups [43]:

1. **Zero invariants:** Some AMIs may be identically zero regardless of the image from which they are calculated.
2. **Products:** Some invariants may be products of other invariants.
3. **Linear combinations:** Some invariants may be linear combinations of other invariants.
4. **Identical invariants**
5. **Polynomial dependencies:** if there exists a finite sum of products of invariants (including their integer powers) that equals zero, the invariants involved are polynomially dependent.

The invariants having the dependencies 1 to 4 are called reducible invariants. After eliminating all of them, we obtain a set of so-called *irreducible* invariants. However, irreducibility does not mean independence. Since the discussion about detect reducible and polynomially dependent invariants is beyond the scope of this work, interested reader is referred to more detailed discussion in [43]. The authors list all independent AMIs up to the weight 12 (80 independent invariants out of 1589 irreducible invariants), which we are going to use in our work.

CHAPTER 5

5. PROPOSED FINGERPRINT MATCHING ALGORITHM

5.1 Directional Filtering and Feature Extraction

A fingerprint consists of a series of ridges that mainly flow parallel to the locally dominant direction and occasionally make local singularities, like a core or delta point. Since fingerprint patterns have strong directionality, directional information can be exploited as fingerprint features. In this sense, a DFB is suitable for extracting the features of fingerprints containing many linear and directional components, because it can effectively and accurately decompose an image into several directional sub-band outputs.

For feature extraction, the original fingerprint image is decomposed into eight directional sub-band outputs using the DFB, and the moment invariants to translation, rotation, and scaling and affine moment invariants

(independent and irreducible) of each block can be obtained from the decomposed sub-band outputs. Let $f_{\theta}(x, y)$ denote the coefficient at position (x, y) of sub-band θ corresponding to a region of interest (ROI) image block B . Where $\theta \in \{0, 1, 2, \dots, 7\}$ for the sub-bands.

For an $N \times N$ image, the first half of the eight sub-band outputs is $N/4 \times N/2$ in size, while the other half is $N/2 \times N/4$, as explained in Section 4.5. Therefore, the sub-bands corresponding to an $m \times n$ block have size $m/4 \times n/2$ for directions 0 to 3, and size $m/2 \times n/4$ for directions 4 to 7, as illustrated in Figure 5.1.

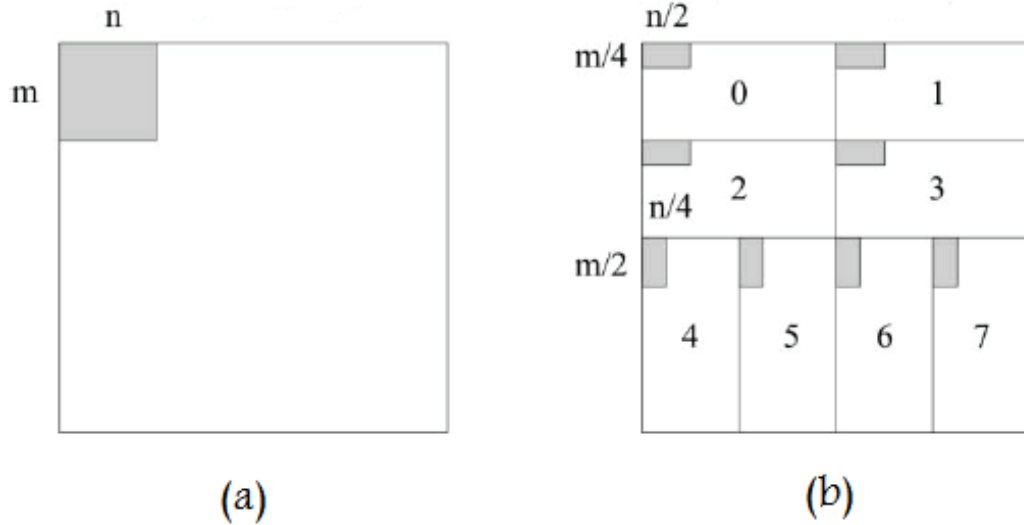


Figure 5.1: blocks in (a) Original image, (b) Sub-band output.

The proposed scheme of feature extraction first locates a reference point and establishes an ROI around the detected reference point. The established ROI is then decomposed into eight directional sub-band outputs using a DFB.

Finally, the fingerprint feature values based on moment invariants (TRS & AMIs) are calculated from each sub-block of the decomposed sub-band outputs.

5.2 Image Normalization

The objective is to decrease the dynamic range of the gray between ridges and valleys of the image. We normalize the image to constant mean and variance. Normalization is done to remove the effects of sensor noise and finger pressure difference. Let $I(i, j)$ denotes the gray value at pixels (i, j) . M and VAR are the estimated mean and variance of the input fingerprint image. We used FBI WSQ standard for gray scale images:

$$I'(i, j) = \frac{I(i, j) - M}{VAR'} \quad (23)$$

Where $VAR' = VAR/128$ for 8-bits of precision per pixel.

5.3 *Reference Point and Region of Interest*

4.3.1 Determination of Reference point

The reference (core) (Figure 5.2) point is defined as “the point of the maximum curvature on the convex ridge [45],” which is usually located in the central area of fingerprint. A summary of reference point location algorithm is presented below [15].



Figure 5.2: The reference point one on the convex ridge.

1. Estimate the orientation field O using a window size of $w \times w$.
2. Smooth the orientation field in a local neighborhood. Let the smoothed orientation field be represented as O' . In order to perform smoothing (low-pass) filtering, the orientation image need to be converted into a continuous vector field, which is defined as:

$$\Phi_x(i, j) = \sum_{u=-w_\Phi/2}^{w_\Phi/2} \sum_{v=-w_\Phi/2}^{w_\Phi/2} W(u, v) \cdot \Phi_x(i - uw, j - vw) \quad (24)$$

$$\Phi_y(i, j) = \sum_{u=-w_\Phi/2}^{w_\Phi/2} \sum_{v=-w_\Phi/2}^{w_\Phi/2} W(u, v) \cdot \Phi_y(i - uw, j - vw) \quad (25)$$

Where W is a two-dimensional low-pass filter with unit integral and $w_\Phi \times w_\Phi$ specifies the size of the filter.

3. Compute ε , an image containing only the sine component of O' .
4. Initialize A , a label image used to indicate the reference point.
5. For each pixel (i, j) integrate pixel intensities (sine component of the orientation field).
6. Find the maximum value and assign its coordinate as the reference point.

4.3.2 Determination of ROI and Partition

After determining the coordinates of the reference point we crop the fingerprint image into an ROI. In order to speed up the overall process, we use only a predefined square area (ROI) with size $N \times N$ around the reference point at the center for feature extraction instead of using the entire fingerprint. In our experiment, we set N to 192. The center of the cropped

image centers the position of the reference point. Figure 5.3 demonstrates the ROI centered on the determined reference point of two input fingerprints, respectively.

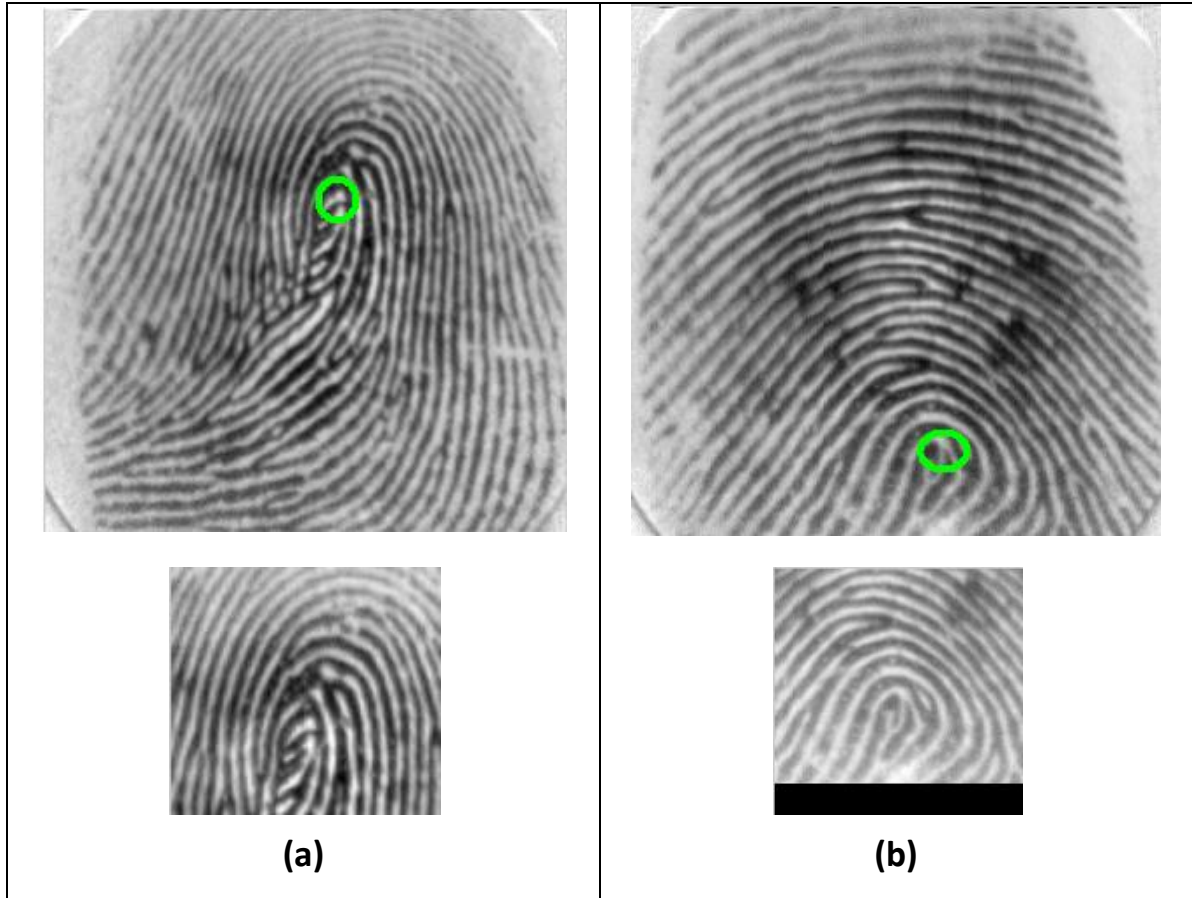


Figure 5.3: Region of interest (ROI) for feature extraction. A sample fingerprint (a) whose ROI is established within the image and (b) whose ROI exceeds the image bound.

In case that the detected reference point is located at the corner of the image as shown in Figure 5.3 (b), establishing the ROI of a fingerprint exceeds the bound of an image. In such a case, the proposed method sets up the ROI by

inserting zeros in the outside area of the image. The ROI area with zero value is excluded when fingerprint features are calculated and matching is performed.

5.4 Invariant Moment Feature Vector Generation

At this stage, we apply the invariant moment analysis introduced in Section 4.9 and 4.10 on each one of the eight sub-band respectively. The extracted ROI as shown in Figure 5.3 is decomposed into eight directional sub-band outputs by an eight-band DFB. For each sub-band, divide it into sub-blocks and a set of 35 independent AMIs and 21 TRS moment invariants of the 5th order is computed for each sub-block. As a result 56 set of invariant moments for each of the 8 sub-blocks are extracted as features to represent a fingerprint.

The procedure for feature extraction can be summarized as follows:

1. Normalize the image.
2. Identify the core point and extract the ROI.
3. Apply the eight-band DFB to the ROI with dimension $N \times N$. The output is a set of eight subbands as illustrated in Figure 3.2 (d).

4. Further divide each sub-band output into sub-blocks that will serve as the region of support for the feature vector calculations. If we envision a sub-block of size $n \times n$ (where N is a multiple of n) then the sizes of the corresponding sub-blocks with the sub-bands are $n/4 \times n/2$ for sub-bands 0 to 3 and $n/2 \times n/4$ for sub-bands 4 to 7.
5. Calculate the 56 set of invariant moments from each “smaller block” to form the feature vector, as introduced in sections 4.9 and 4.10.
6. Finally, combine the features calculated from each sub-block $I_{\theta k}$ into one vector $V_f = \{I_{01}, I_{02}, \dots, I_{\theta k}\}$, where $\theta \in \{0, 1, 2, 3, 4, 5, 6, 7\}$ and $k \in \{0, 1, 2, \dots, 56\}$.

5.5 Fingerprint Matching

Generally speaking, other methods require that before the input print and template print are compared with each other, they should be translationally and rotationally aligned with each other. Rotational alignment is achieved by generating cyclical input feature vectors and matching input feature vectors with template feature vectors. In our proposed method, the translational alignment is not of concern because by applying invariant analysis to the extracted ROI by the reference point detection process. Since the proposed

feature extraction process is based on moments that are invariant to translation, rotation and scaling, the proposed method is robust to angular deviations without rotation and translation compensation.

Fingerprint matching is performed based on finding the absolute distance between the input feature vectors and the template feature vector enrolled in the database. Let:

$$V_{f1} = \{a_1, a_2, \dots, a_n\} \quad \text{and} \quad V_{f2} = \{b_1, b_2, \dots, b_n\} \quad [26]$$

Denote the feature vectors of the two fingerprints to be matched, the difference vector V_d of the two fingerprint feature vectors is calculated as in (27).

$$V_d = \left(\frac{|a_1 - b_1|}{\max(|a_1, b_1|)}, \frac{|a_2 - b_2|}{\max(|a_2, b_2|)} \dots \dots \frac{|a_n - b_n|}{\max(|a_n, b_n|)} \right) \quad (27)$$

We define the absolute distance of the two matching vectors as in (28).

$$R_m = \sum_{i=1}^n \frac{|a_i - b_i|}{\max(|a_i, b_i|)} \quad (28)$$

CHAPTER 6

6. EXPERIMENTAL RESULTS

We used moment analysis to extract invariant features from partitioned DFB sub-images in an ROI.

In order to measure the objective performance, we run the matching algorithm on images from FVC2002 fingerprint database set, which contains four distinct databases: DB1_A, DB2_A, DB3_A and DB4_A. Each database consists of 800 images (100 distinct fingers, 8 impressions each). In order to obtain the performance characteristic such as EER (Equal Error Rate) we perform a total of 2,800 genuine comparisons (each instance of a finger is compared with the rest of the instances resulting in $(8 \times 7)/2$ tests per finger) and 39,600 impostor comparisons (the first instance of each finger is compared against the first instance of all other fingers resulting in a total of $(100 \times 99)/2$ tests for each impression).

Number of Genuine Tests	Number of Impostor Tests
2,800	39,600

Table 6.1: Number of Tests.

First, the genuine and imposter distributions were obtained for the proposed method, then the verification performance was assessed based on the characteristics of the distributions. The genuine distribution indicates the distribution of the distances between all possible intra-class image pairs in the database, while the imposter distribution represents the distribution of the distances between all possible inter-class image pairs in the database. The more the genuine and imposter distributions are separated and the smaller the standard deviation for each distribution, the more advantageous for a personal verification method. Figure 6.1 shows the genuine and imposter distributions for the proposed method along with their characteristics in Table 6.2.

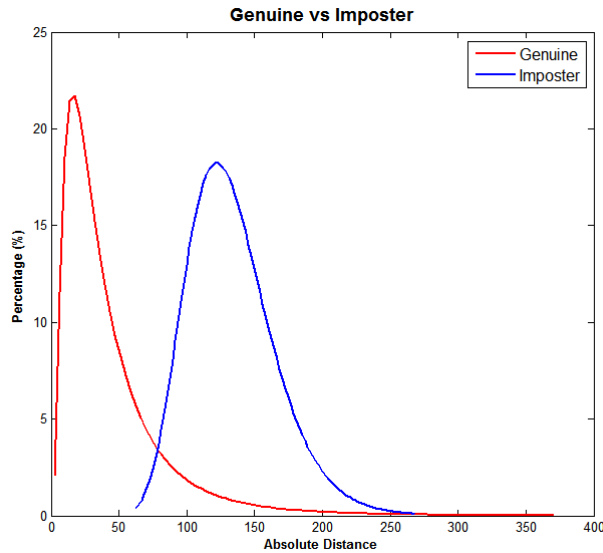


Figure 6.1: Genuine and imposter distributions for the proposed method (DB1_A).

Genuine Distribution		Imposter Distribution	
Mean	Variance	Mean	Variance
12.2	2.5	22.8	3.8

Table 6.2: Statistical characteristics of genuine and imposter distributions (DB1_A).

The performance of a verification method is often estimated using the false accept rate (FAR) and false reject rate (FRR). Here, FAR is the rate at which an imposter print is incorrectly accepted as genuine and FRR is the rate at which a genuine print is incorrectly rejected as an imposter. The FRR and FAR are defined as follows:

$$FRR = \frac{\text{Number of rejected genuine claims}}{\text{Total number of genuine accesses}} \times 100\% \quad (29)$$

$$FRR = \frac{\text{Number of accepted imposter claims}}{\text{Total number of imposter accesses}} \times 100\% \quad (30)$$

The EER is used as a performance indicator. The EER indicates the point where the FRR and FAR are equal. Table 6.2 shows performances of our proposed method over the four databases of FVC2002. From the tables, we can find that the average EER values of absolute distance matching and that of over four databases are 4.91%. The table shows that DB2_A has the highest EER of 6.21% and this is due to the poor quality of the fingerprint images in that set.

Database	EER (%)
DB1_A	3.35
DB2_A	6.21
DB3_A	5.78
DB4_A	4.28
Average	4.91

Table 6.3: Testing results.

The performance of a verification system can also be evaluated using a receiver operator characteristic (ROC) curve, which graphically demonstrates how the correct acceptance rate ($CAR = 1 - FRR$) changes with a variation in FAR. Here, the CAR indicates the rate at which a genuine print is correctly accepted as genuine. In order to examine the performance of the proposed method, a number of experiments comparing performance to other method were carried out on the FVC2002 database. Two matching methods, proposed in references [15, 26] were selected for comparison, namely, filter bank approach matching using Gabor filters and Directional filter (DFB). Figure 6.2 shows the ROC curve for the proposed method outperform the others.

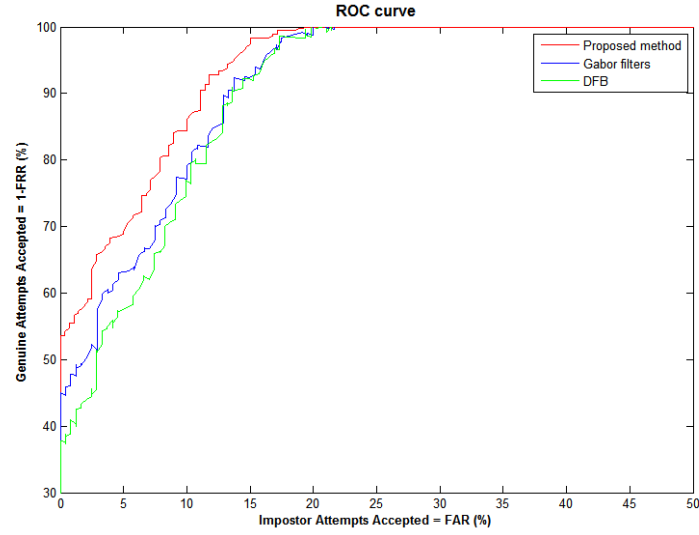


Figure 6.2: ROC curves comparing the recognition rate performance of the proposed method with the other 2 methods on database FVC2002 DB1_A.

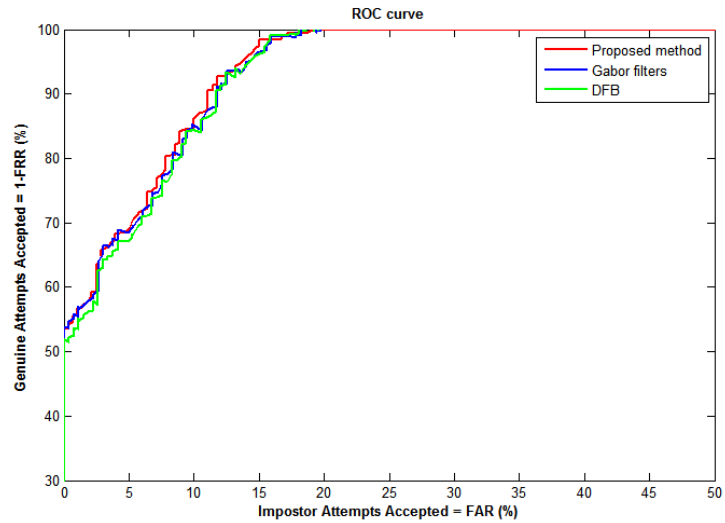


Figure 6.3: ROC curves on database FVC2002 DB2_A.

As shown previously that DB2_A has the highest EER, Figure 6.3 shows how the ROC curves gives mixed results due to the poor quality of the fingerprint images in that set. Figures 6.4 and 6.5 confirms that the proposed

method gives better performance on FVC2002 DB3_A and DB4_A, as the results presented from the first database set. It is noted that DFB method outperformed the Gabor Filter method only on DB3_A, as illustrated in Figure 6.4.

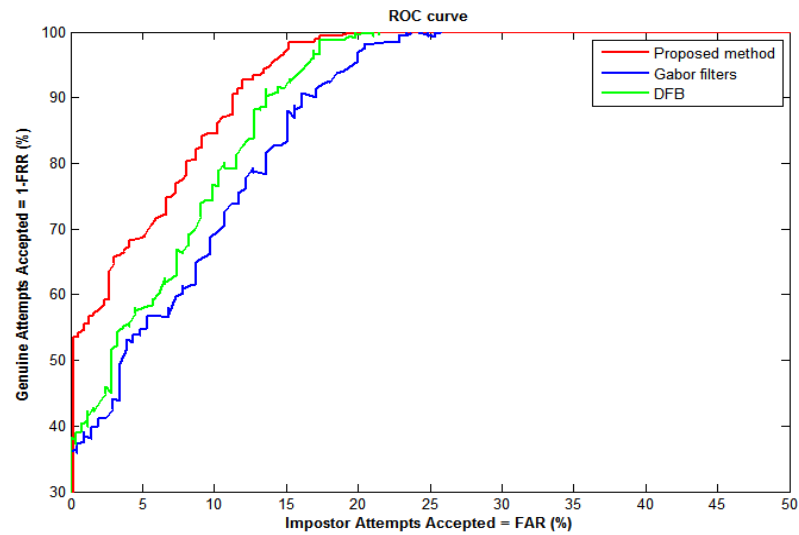


Figure 6.4: ROC curves on database FVC2002 DB3_A.

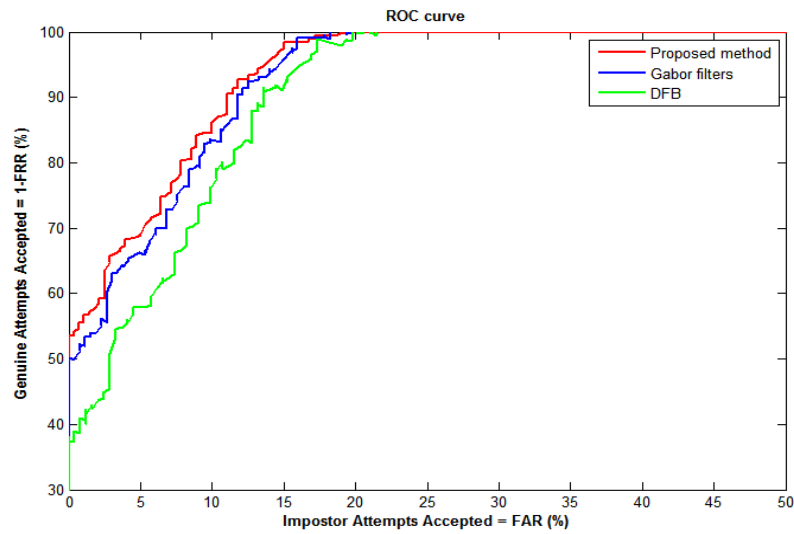


Figure 6.5: ROC curves on database FVC2002 DB4_A.

The proposed method has better verification accuracy to the other leading techniques as Table 6.3 shows. However, Table 6.4 shows that the other methods used as benchmark have the advantage of speed, in terms of processing time needed for feature extraction. Another advantage over the proposed method was the memory size for the feature vector. Finally, comparison time is the same for the proposed method and DFB, with Gabor filter method being last due to the sector by sector comparison.

	Processing time	Comparison time	Memory size
Proposed Method	0.533 sec	0.03 sec	583 bytes
DFB	0.358 sec	0.03 sec	225 bytes
Gabor Filter	0.479 sec	0.1 sec	440 bytes

Table 6.4: Time & memory comparison.

CHAPTER 7

7. CONCLUSION

7.1 *Overview*

This work presented a fingerprint matching algorithm that combines AMIs and TRS invariants based on moments analysis that does not have to detect minutiae. First, a preprocessing by normalizing the fingerprint image using WSQ standard definition is done.

The reference point can be reliably and accurately determined with the analysis of orientation field. Then uses the area within a certain range around the detected reference point as a ROI for feature extraction.

The method uses a DFB to obtain directional components of the image. Using the invariant moment analysis on sub-bands of the filtered images, the extracted features have bound the effects of noise and non-linear distortions, while utilizing the invariant ability to the translation, rotation, scaling and affine transformations of features to handle various input

conditions. The new feature vector capture more global information on fingerprint ridges pattern.

Matching the fingerprints is implemented by absolute distance which has a faster matching speed than other methods. This is because of the nature of the AMIs and TRS invariants used that eliminate the translational and rotational alignment to be done.

Experimental results using FVC2002 fingerprint database demonstrate that the proposed method has better verification accuracy to the other leading techniques, along with robustness to image rotation and translation. We present the comparative results in Table 6.2. The improvement in the ROC curves presented in the experimental results section.

7.2 Summary of Contributions

The proposed method has better verification accuracy to the other leading techniques, along with robustness to image rotation and translation. However the other methods used as benchmark have the advantage of speed, in terms of processing time needed for feature extraction. Another advantage over the proposed method was the memory size for the feature vector.

7.3 *Future Work*

A number of opportunities exist to extend this work. First, an investigation to other moments family like Zernike, Orthogonal Fourier–Mellin, Legendre, and Chebyshev moments, examining their potential to be used to construct a feature vector and the discriminate power they can achieve. Second, exploring the use of other transform like curvelets and contourlet. Finally, considering the use of a hybrid-classifier to seek improving the accuracy of matching.

8. REFERENCES

- [1] A. K. Jain, P. Flynn, and A. A. Ross. *Handbook of Biometrics*. Springer, 2009.
- [2] International Biometric Group. Biometric statistics in focus. Elsevier Ltd., 2006.
- [3] International Biometric Group. Biometrics Market and Industry Report. Elsevier Ltd., 2009.
- [4] Acuity Market Intelligence. The Future of Biometrics 2009.
- [5] D. Maltoni, D. Maio, A. K. Jain, and S. Prabhakar. *Handbook of Fingerprint Recognition*. Springer, 2009.
- [6] U. Park, S. Pankanti, and A. K. Jainban, “*Fingerprint Verification Using SIFT Features*,” SPIE Defense and Security Symposium, Orlando, Florida, 2008.
- [7] S. Yang, and I. M. Verbauwhede, “*A secure fingerprint matching technique*,” Proceedings of the 2003 ACM SIGMM workshop on Biometrics methods and applications, Berkley, California, November 08, 2003.
- [8] A. K. Jain, L. Hong, and S. Pankanti, “*Biometric identification*,” Comm. ACM, pp. 91–98, 2000.
- [9] X. Jiang, and W. Yau, “*Fingerprint minutiae matching based on the local and global structures*,” Proceedings 15th International Conference on Pattern Recognition. (ICPR-2000). IEEE Comput. Soc. Part, vol. 2, pp. 1038-41, Los Alamitos, CA, USA, 2000.
- [10] L. Hong, Y. Wan, and A. Jain, “*A Fingerprint Image Enhancement Algorithm and Performance Evaluation*,” IEEE Trans. on Pattern Analysis and Machine Intelligence, vol. 20, no. 8, pp. 777-789, 1998.

- [11] N. K. Ratha, J. H. Connell, and R. M. Bolle, "*An Analysis of Minutiae Matching Strength*," Lecture Notes in Computer Science, vol. 2091, pp. 223-228, 2001.
- [12] FVC2002, <http://bias.csr.unibo.it/fvc2002/>
- [13] S. Chikkerur, S. Pankanti, A. Jea, N. Ratha, and R. Bolle, "*Fingerprint Representation Using Localized Texture Features*," International Conference on Pattern Recognition, pp. 521-524, 2006.
- [14] D. Lowe, "*Distinctive image features from scale-invariant key points*," International Journal of Computer Vision, vol. 60, no. 2, pp. 91-110, 2004.
- [15] A. K. Jain, S. Prabhakar, L. Hong, and S. Pankanti, "*Filterbank-based Fingerprint Matching*," IEEE Trans. on Image Processing, vol. 9, no. 5, pp. 846-859, 2000.
- [16] X. Feng, Tong, X. Long, J. Huang, and X. Li. "*Fingerprint minutiae matching based on complex minutiae vector*," In Proceedings of International Conference on Machine Learning and Cybernetics, vol. 6, pp. 3731, 2004.
- [17] X. Liang, and Asano, "*Fingerprint matching using minutia polygons*," In 18th International Conference on Pattern Recognition (ICPR), vol. 1, pp. 1046-1049, 2006.
- [18] A. Ross, A. Jain, and J. Reisman, "*A Hybrid Fingerprint Matcher*," International Conference on Pattern Recognition (ICPR), Quebec City, August 11-15, 2002.
- [19] R. O. Duda and P. E. Hart, "*Generalizing the Hough transform to detect arbitrary shapes*," Pattern Recognition vol.3, no. 2, pp.110-122, 1981.
- [20] K. Fielding, J. Homer, and C. Makekau, "*Optical fingerprint identification by binary joint transform correlation*," Optical Engineering, vol. 30, no. 12, 1992.
- [21] F. T. Gamble, L. M. Frye, and D. R. Grieser, "*Real-time fingerprint verification system*," Applied Optics, vol. 31, no. 5, pp. 652-655, 1992.

- [22] V. Govindaraju, Z. Shi, and J. Schneider, “*Feature extraction using a chain-coded contour representation*,” Proc. Int. Conf. on Audio- and Video-Based Biometric Person Authentication.
- [23] A. N. Marana and A. K. Jain, “*Ridge-based fingerprint matching using hough transform*,” In 18th Brazilian Symposium on Computer Graphics and Image Processing (SIBGRAPI05), pp. 112-119, 2005.
- [24] A. Ross, S. C. Dass, and A. K. Jain, “*Fingerprint warping using ridge curve correspondences*,” Pattern Analysis and Machine Intelligence, IEEE Trans. pp. 19-30, 2006.
- [25] S. K. Oh, J. J. Lee, C. H. Park, B. S. Kim, and K. H. Park, “*New Fingerprint Image Enhancement Using Directional Filter Bank*,” Journal of WSCG, vol. 11, no. 1, 2003.
- [26] C. H. Park, J. J. Lee, and M. J. Smith, “*Directional Filter Bank-Based Fingerprint Feature Extraction and Matching*,” IEEE Transactions on Circuits and Systems for Video Technology, vol. 14, no. 1, pp. 74-85, 2004.
- [27] O. A. Zuniga and R. M. Haradick, “*Integrated Directional Derivative Gradient Operators*,” IEEE Trans. Systems, Man, and Cybernetics, SMC-17, pp. 508-517, 1987.
- [28] G. Iannizzotto and F. La Rosa, “*A SIFT-Based Fingerprint Verification System Using Cellular Neural Networks*,” Pattern Recognition Techniques, Technology and Applications. pp. 626, 2008.
- [29] M. M. Mokji, S. A. S. Abu Bakar, and Z. Ibrahim, “*Fingerprint Classification Based on Directional Image Constructed Using Wavelet Transform Domains*,” International Conference on Robotics Vision, Information, and Signal Processing (ROVISP 2003), Penang, Malaysia, pp. 22-24, January 2003.
- [30] W. K. Lee and J. H. Chung, “*Automatic real-time identification of fingerprint images using wavelets and gradient of Gaussian*,” 40th Midwest Symposium on Circuits and Systems, Vol. 2, pp. 917-920, 1997.

- [31] M. Antonini, M. Barlaud, and P. Mathieu, "*Image Coding using Wavelet Transform*," IEEE Trans. on Image Processing, vol. 2, no. 2, pp. 205-220, 1992.
- [32] M. M. Mokji, S. A. S. Abu Bakar, and Z. Ibrahim, "*Fingerprint Classification Using Signature Obtain From Second Stage Discrete Wavelet Transform*," Malaysian Science and Technology Congress on Information and Communication Technology, Penang, Malaysia, November 2001.
- [33] Jea, T. Minutiae-based partial fingerprint recognition. Ph.D. thesis, State University of New York at Buffalo, 2005.
- [34] B. D. Patil, J. V. Kulkarni, and R. S. Holambe, "*Fingerprint Verification Using Wavelet and Local Dominant Orientation*," Visual Information Engineering, 2006. VIE 2006. IET International Conference, pp. 79-82, 2006.
- [35] D. Lowe, "*Method and apparatus for identifying scale invariant features in an image and use of same for locating an object in an image*," U.S. Patent 6,711,293.
- [36] D. Lowe, "*Object recognition from local scale-invariant features*," Proceedings of the International Conference on Computer Vision, pp. 1150–1157, 1999.
- [37] R. M. Rao, and A. S. Bopardikar. *Wavelet Transforms: Introduction to Theory & Applications*. Prentice Hall, 1998.
- [38] J. C. Goswami. *Fundamentals of Wavelets: Theory, Algorithms, and Applications*. Wiley-Interscience, 1999.
- [39] M. N. Do and M. Vetterli, "*Pyramidal directional filter banks and curvelets*," IEEE International Conference on Image Processing (ICIP), Thessaloniki, Greece, October 2001.
- [40] R. H. Bamberger and M. J. T. Smith, "*A filter bank for the directional decomposition of images: Theory and design*," IEEE Trans. Signal Processing, vol. 40, pp. 882–893, Apr. 1992.

- [41] M. N. Do and M. Vetterli, “*The contourlet transform: an efficient directional multiresolution image representation*,” IEEE Trans. Image on Processing, vol. 14, no. 12, pp. 2091-2106, December 2005.
- [42] M. N. Do and M. Vetterli. *Contourlets, Beyond Wavelets*. G. V. Welland ed., Academic Press, 2003.
- [43] J. Flusser, T. Suk, and B. Zitova. *Moments and Moment Invariants in Pattern Recognition*. Jon Wiley & Sons, 2009.
- [44] S. Park, M. J. T. Smith, and R. M. Mersereau, “*A new directional filter bank for image analysis and classification*,” in Proc. Int. Conf. Acoustics, Speech, and Signal Processing, vol. 3, 1999, pp. 1417–1420.
- [45] M. Liu, X. D. Jiang, and A. Kot, “*Fingerprint reference-point detection*,” EURASIP Journal on Applied Signal Processing, vol. 2005, no. 4, pp. 498-509, 2005.
- [46] S. Pankati and M. M. Yeung, “*Verification Watermark on Fingerprint Recognition and Retrieval*,” SPIE, Security and Watermarking of Multimedia Contents, vol. 3657, pp. 66-78, April 1999.

Vita

Personal

Information

- Date of Birth: 1981
- Place of Birth: KSA
- Nationality: Saudi
- Email: <mailto:Waleedyyy@gmail.com>
- Mobile #: +966-504817818
- Present Address: Menna Street, Mazroayiah District, P.O.BOX 35122, ZIP 31488, Dammam, Saudi Arabia.
- Permanent Address: Menna Street, Mazroayiah District, P.O.BOX 35122, ZIP 31488, Dammam, Saudi Arabia.
- Languages:
 - 1. Arabic (native language)
 - 2. English

Education

- 1999 -2004: King Fahd University of Petroleum & Minerals, Dhahran, Bachelor of Science in Software Engineering.
- 2005-2006: New York Institute of Technology, Master of Business Administration.
- 2007-2010: King Fahd University of Petroleum & Minerals, Dhahran, Master of Science in Computer Science.

Work

- 2005- March 2010: Analyst, Saudi Electricity Company.

Interests

- Image processing and pattern recognition
 - Biometric systems
 - Software architecture
 - ERP systems
-